International Journal of Hydrogen Energy 98 (2025) 1492–1509

Contents lists available at ScienceDirect

International Journal of Hydrogen Energy

journal homepage: www.elsevier.com/locate/he

Effective catalysts for typical liquid organic hydrogen carrier *N*-Ethylcarbazole

Preetham Permude [a], Chunguang Tang [b,*], Adnan Ahmad [a], Hua Chen [a], Terry Frankcombe [c,**], Yun Liu [a,***]

[a] Research School of Chemistry, The Australian National University, Canberra, ACT, 2601, Australia
[b] Institute for Frontier Materials, Deakin University, Geelong, VIC, 3220, Australia
[c] School of Science, The University of New South Wales, Canberra, ACT, 2601, Australia

ARTICLE INFO

Handling Editor: Dr Mehran Rezaei

Keywords:
Liquid organic hydrogen carrier
N-ethylcarbazole
Hydrogen storage
Catalyst

ABSTRACT

Hydrogen can play a significant role as a clean energy vector due to its abundance, high gravimetric energy density, and environmental friendliness. However, efficient hydrogen storage remains a bottleneck that poses economic and technological challenges to the current system. Liquid organic hydrogen carriers (LOHCs) have drawn intensive attention for their excellent compatibility with the existing fuel infrastructure. Among the LOHCs under development, *N*-ethylcarbazole (NEC) is an attractive option mainly due to its ability to undergo hydrogenation and dehydrogenation below 200 °C. This review discusses the recent experimental and theoretical progress of catalyst development for hydrogen storage in NEC. The effect of various catalysts, including Ru-, Ni-, Pd-, and Pt-based, on (de) hydrogenation of NEC is discussed. In addition, bidirectional catalysts and catalyst support materials are also discussed. We conclude the review with a brief discussion of the future research directions.

1. Introduction

The increase in energy consumption and depletion of traditional energy sources have prompted the global shift to renewable energy sources. Evolving geopolitical conditions and the effects of climate change have further added to the demand for renewable energy. Compared to conventional non-renewable fuels, hydrogen has a high heating value (fuel energy content) by mass and other favourable properties, such as being environmentally friendly and regenerative [1]. Along with this, hydrogen has the potential to be efficient, versatile, and cost-effective [2]. For the application of hydrogen as fuel, efficient storage is a significant criterion, and in the case of hydrogen, storage can be classified into two approaches. The physical approach includes compressed gas cylinders (up to 800 bar), hydrogen liquefication (~-252 °C), and adsorption of hydrogen in porous materials (~-173 °C) [3]. The chemical approach includes the storage of hydrogen as (complex) metal hydrides, amides [3], liquid organic hydrogen carriers (LOHCs) [4] and ammonia-based hydrogen carriers [5].

Compared to its excellent gravimetric energy density (120 MJ/kg), hydrogen has a low volumetric energy density, 0.01 MJ/L (at 1 atm and 25 °C) [6], which has hindered hydrogen's large-scale application as fuel. Compression and liquefication do not improve the situation significantly [7]. For existing technical applications, hydrogen is stored as liquid hydrogen (LH_2) at a low temperature, around ~ -252 °C, with an energy density of ~10 MJ/L, or as compressed gaseous hydrogen (CGH_2, up to 700 bar) [8] with the density around 5.6 MJ/L at 700 bar [9]. Under the current technological conditions, based on a lower heating value of 120 MJ/kg, LH_2 uses 30% of stored energy for liquefaction, whereas it costs 15% for CGH_2 to achieve 700 bar compression [10]. For cryogenic liquid H_2, the evaporation of liquid and the cost of liquefaction prove to be a significant barrier. Compressed H_2 would have considerable safety, weight, and cost issues for large-scale applications as the tank's pressure and size increase.

Along with the technological complexity of storing hydrogen, there is a need to develop an international distribution system to encourage hydrogen uptake. The storage and distribution system should also consider the problem of hydrogen embrittlement (HE) of metals, where

* Corresponding author.
** Corresponding author.
*** Corresponding author.
E-mail addresses: chunguang.tang@deakin.edu.au (C. Tang), t.frankcombe@unsw.edu.au (T. Frankcombe), yun.liu@anu.edu.au (Y. Liu).

https://doi.org/10.1016/j.ijhydene.2024.12.038
Received 1 October 2024; Received in revised form 21 November 2024; Accepted 2 December 2024
Available online 20 December 2024

Abbreviations

LOHCs	liquid organic hydrogen carriers
NEC	*N*-ethylcarbazole
CGH_2	Compressed gaseous hydrogen
LH_2	Liquid hydrogen
HE	Hydrogen embrittlement
MTH	Methylcyclohexane-toluene-hydrogen
4H-NEC	tetrahydro-NEC
8H-NEC	octahydro-NEC
DME	Dimethylether
XPS	X-ray photoelectron spectroscopy
NP	Nanoparticle
rGO	Reduced graphene oxide
AC	Activated carbon
COM	Commercial catalyst
CR	Chemically reduced
SiCN	Silicon carbon nitride
ARC	Australian Research Council

fracture initiation, subcritical crack growth, and catastrophic failure with subsequent loss of mechanical properties are possible due to electrochemical reactions and high-pressure hydrogen gas environments [11]. Hence, the need to store hydrogen in chemical compounds that can undergo storage cycles is gaining importance [12–19]. Ethanol and Ammonia are attractive options due to their compatibility with existing liquid fuel infrastructure, but their decomposition and synthesis are capital and energy-intensive [20]. Hence, storing hydrogen via LOHCs has been proposed as an attractive option.

LOHC systems consist of hydrogen-lean and hydrogen-rich pairs that store hydrogen using catalytic hydrogenation and dehydrogenation cycles with the help of catalysts, as shown in Fig. 1. The system can be coupled with a renewable energy source, which produces electricity, that can produce hydrogen (H_2) using H_2O electrolysis [21]. The produced H_2 can be used to convert hydrogen-lean molecules to hydrogen-rich molecules. The hydrogen-rich molecules can be stored and transported to release H_2 on request to generate electricity using a fuel cell. The entire system has the potential to play a significant role in satisfying our energy demand. LOHCs do not require cryogenic tanks or high-pressure vessels for transporting hydrogen and can store 6–8 wt% hydrogen at ambient conditions. Due to the chemical similarity of LOHCs to gasoline and diesel, large-scale transportation along with low maintenance cost is possible with the help of existing petroleum transportation and processing infrastructure [10]. Also, compared with other storage methods, storing hydrogen via LOHCs has many advantages, such as being economical, compatible with present infrastructure, ambient conditions for transport, and clean and leak-free [4,22].

The exploration of hydrogen storage in organic molecules started over forty years ago [23,24], with the first mention of hydrogen storage in organic molecules appearing in the technical report of Exxon Company [25]. The 1980s saw significant contributions to this field from Italy [26], Switzerland [27], and Canada [28], leading to the popularisation of the term 'liquid organic hydride' [24]. In 1981, the Paul Scherrer Institute proposed using liquid organic carrier MTH (methylcyclohexane-toluene-hydrogen) as a fuel [27]. The team suggested prototype trucks and investigated the technical and economic feasibility of hydrogen combustion engines [23,29,30].

Approximately two decades later, Air Products proposed heterocyclic organic hydrogen carriers due to their potential to dehydrogenate the molecules at lower reaction temperatures [24,31], as depicted in Fig. 3. They found that materials with high hydrogenation enthalpies require high temperatures for their dehydrogenation reactions, whereas those with low hydrogenation enthalpies are not stable [32]. Their study noted that the desirable hydrogenation enthalpy range can only be found for materials with large fused aromatic ring systems, as seen in Fig. 3(a). However, the hydrogenation enthalpy can be significantly lowered by substituting nitrogen in the ring, as shown in Fig. 3(b). Later, Eblagon et al. performed comprehensive theoretical and experimental investigation of Ru catalysed hydrogenation for LOHC material *N*-ethylcarbazole and found that low coordination sites can accelerate the conversion of intermediates to fully hydrogenated products [33]. Recently, Fan et al. proposed micropacked bed reactor for continuous hydrogenation of *N*-ethylcarbazole [34]. Fig. 2 illustrates the development of LOHCs and NECs for hydrogen storage for the last six decades.

For effective implementation of LOHC technology, the material must satisfy several criteria along with the hydrogenation enthalpy.

Based on the literature, the selection criteria for LOHC include.

- High gravimetric (>6 wt%) and volumetric (>56 kg/m^3) storage capacities [35].
- Being compatible with current energy infrastructures
- Abundant availability with low production cost and easily recyclable

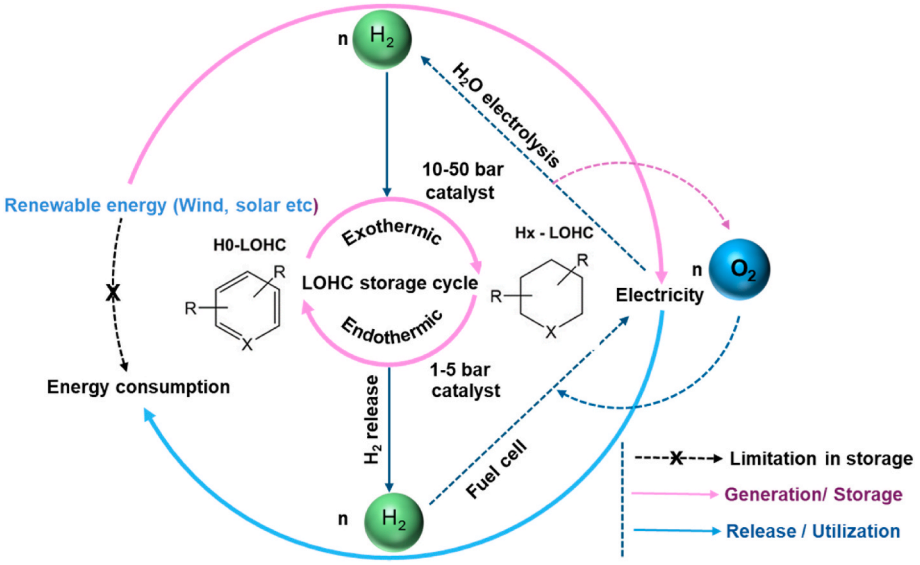

Fig. 1. Catalytic hydrogenation and dehydrogenation cycle of LOHC.

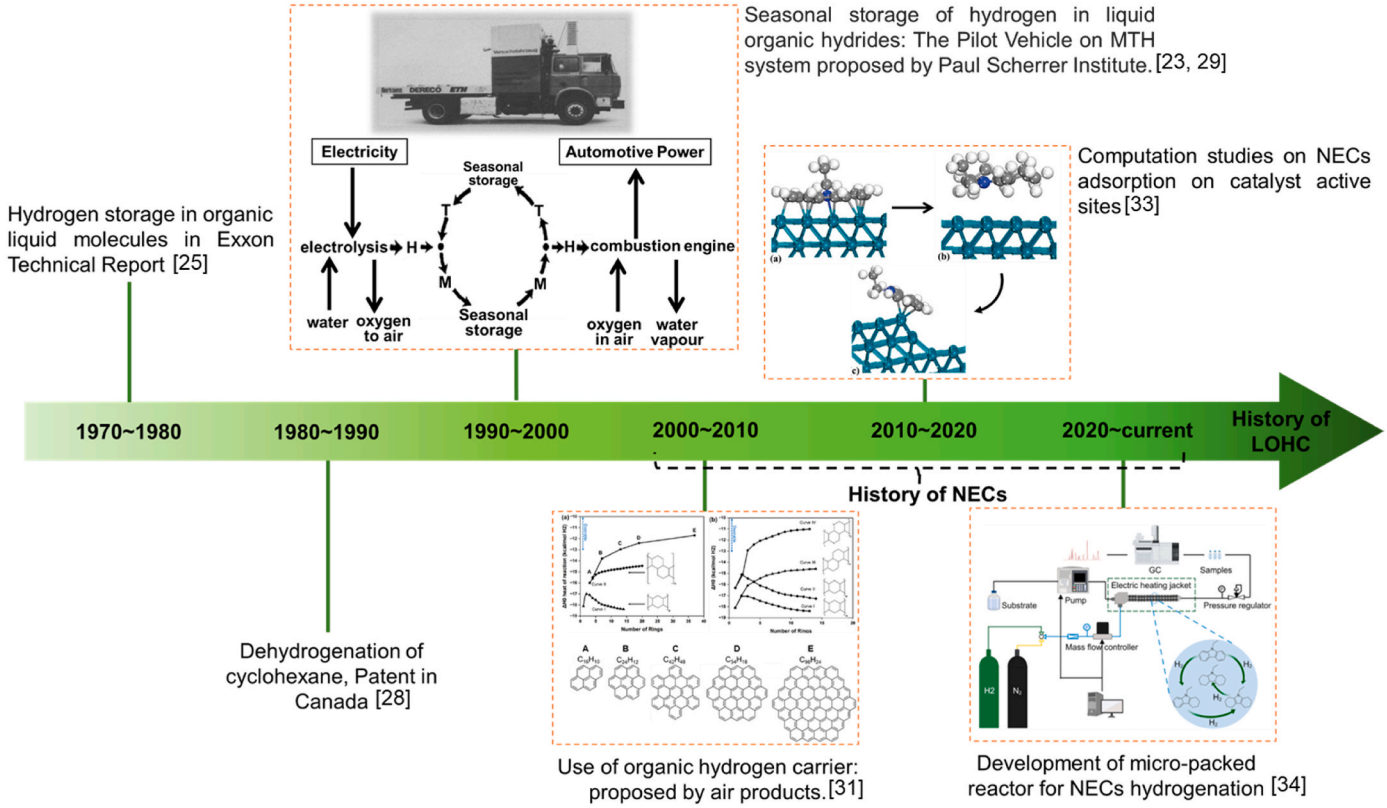

Fig. 2. Timeline development of LOHC and NECs for hydrogen storage.

- Stability upon (de) hydrogenation and transportation
- Low toxicity and high safety
- Suitable liquid temperature range, high boiling point (>300 °C) [35], and high flash point

To date, several LOHC systems, such as *N*-ethylcarbazole, phenazine, dibenzyl toluene, toluene, naphthalene, and 1,2-dihydro-1,2-azaborine have been reported. Their advantages and challenges are listed in Table 1.

While LOHCs are competitive among the hydrogen storage methods, their large-scale applications depend on efficient, economical, and stable catalysts. Among the LOHCs, NEC has been regarded as very promising due to its ideal enthalpy change. Here we aim to review the recent development of catalysts for NEC. This review is structured as follows. Section 2 provides a brief introduction to NEC and its (de)hydrogenation reactions. Section 3 discusses recent advances in catalysts specifically designed for unidirectional hydrogenation or dehydrogenation. In Section 4, we examine studies on support materials. Although these materials are briefly discussed in relation to catalysts in section 3, their specific roles and properties have not been explored. Section 4 aims to provide a more focused analysis on how support materials contribute to catalytic performance. Section 5 explores the latest developments in bidirectional catalysts, a novel approach that enables both hydrogenation and dehydrogenation to occur at the same site. Finally, section 6 outlines promising future directions for research.

2. NEC as a carrier in the LOHC system

Structurally, NEC is obtained by adding an ethyl group to carbazole, which reduces the melting point from 243 °C for carbazole to 68 °C for NEC. The heteroatom in NEC reduces the dehydrogenation enthalpy change, making NEC competitive against other LOHCs. However, the current significant challenges encountered in NEC/12H-NEC include the production of undesirable by-products due to easy thermal alteration of the *N*-ethyl group and the high H_2 pressure required for reverse hydrogenation (68 bar) [56]. To effectively implement NEC as a LOHC, it is essential to know the mechanism of hydrogen storage in NEC. The overall reversible hydrogenation reaction of NEC can be written as

$$C_{14}H_{13}N + 6H_2 \rightleftharpoons C_{14}H_{25}N \quad (1)$$

The detailed hydrogenation and dehydrogenation processes are shown in Fig. 4(a–b). The hydrogenation enthalpy of NEC is −50.6 kJ/mol-H_2, which means the reaction is exothermic [57]. During dehydrogenation, as seen in Fig. 4(b), 8H-NEC is formed due to the preferable removal of hydrogen from the middle ring [36]. In the next step, it either directly forms 4H-NEC, detaching four hydrogen atoms from a side carbon ring, or first forms 6H-NEC and then releases the two hydrogen atoms to form 4H-NEC. In the end, hydrogen-depleted NEC is formed after removing four hydrogen atoms from the other side of the ring. The fully hydrogenated NEC (12H-NEC), partially hydrogenated intermediates like octahydro-NEC (8H-NEC) and tetrahydro-NEC (4H-NEC)) are in the liquid state at room temperature [58], while NEC is solid below 68 °C.

It should be noted that experimentally, 6H-NEC is rarely observed by NMR, and 2H-NEC has never been observed [33,59]. The liquid hydrogenated product offers advantages in terms of transportation due to its ease for pumping, easy storage, and less hazardous nature compared to other technologies such as compressed gas hydrogen, etc. NEC in a solid state is a potential system drawback since it is difficult to pump and transport compared to its hydrogenated product, complicating system operation and design.

To further understand the dehydrogenation process, it is crucial to understand the interaction between reactant and catalyst. Amende et al. showed that at temperatures up to −50 °C, molecular adsorption of 12H-NEC takes place on Pt(111) [59], without molecular decomposition below −100 °C. They also showed that at cryogenic temperatures, 12H-NEC adsorbs molecularly on Pd nanoparticles [40] and Pd(111) [60]. The onset temperature of dealkylation on defect-rich Pt aggregates

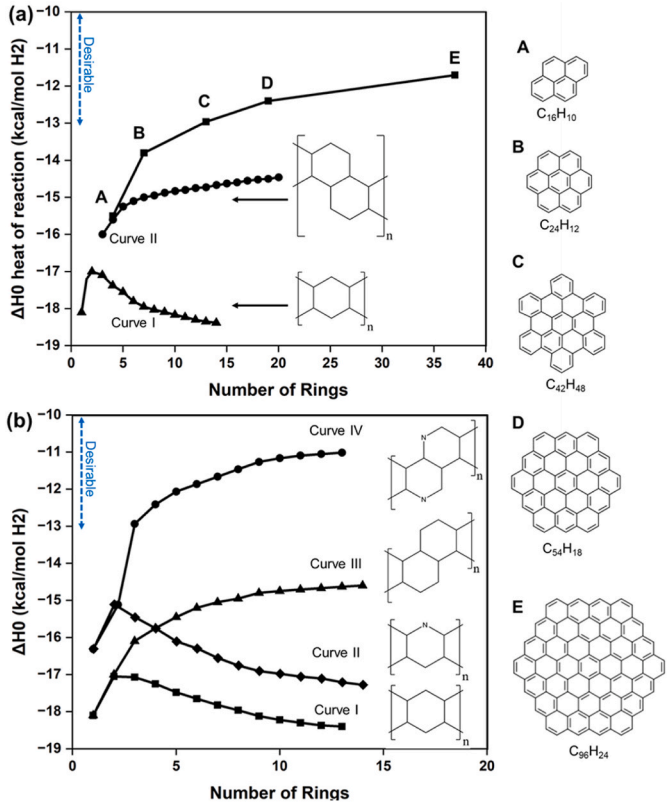

Fig. 3. (a) Calculated hydrogenation enthalpy changes for polyaromatic hydrocarbons versus their structures and the number of rings. (b) Impact of nitrogen heteroatom on calculated hydrogenation enthalpy changes for two isostructural series of polyaromatic hydrocarbons. The enthalpy changes are for standard conditions. Reproduced with permission from Ref. [31].

is about 90 K lower than on single crystal Pt(111) [43], as shown in Fig. 4(c–d). The dealkylation is attributed to easier *N*-ethyl bond breakage triggered by low-coordination Pt sites, whose population increases as the size of Pt particles decreases. Dehydrogenation starts by activating the C–H bond directly near the nitrogen atom in 12H-NEC, resulting in 8H-NEC being the first stable intermediate product. The transition from 12H-NEC to 8H-NEC occurs at temperatures above −50 °C, increasing in rate above 0 °C. Their findings align with computations showing 8H-NEC to be the first intermediate dehydrogenation product [61], a result that we have independently confirmed [62].

Gleichweit et al. conducted in-situ XPS measurement of adsorption and reaction of 12H-NEC on Pt(111) [63]. Their results, highlighted in Fig. 5(a–d), indicate dehydrogenation starts at −73 °C and continues up to 106 °C. Above 116 °C, they observed detrimental reactions where carbon fragments or carbazole are formed on the surface. Their results also support the mechanism that dehydrogenation starts at the carbon atoms next to the nitrogen atom.

The effect of the nitrogen atom and ethyl group on dehydrogenation is two-sided. On the one hand, they were found to promote the dehydrogenation of 12H-NEC by weakening the adsorption to catalyst surfaces, as compared to dodecahydrofluorene and dodecahydrocarbazole [61]. On the other hand, the relatively weak *N*-ethyl bond causes dealkylation, or the scission of the ethyl tail, which hampers the functioning in the long run, for example, by increasing the melting point of the molecule. Dealkylation on Pt (111) was observed above 116.85 °C [59,64], with 8H-carbazole being the primary desorbed product, followed by 8H-NEC. The breakage of ethyl tail at high temperatures to smaller molecular fragments is similar to the pathway taken by other hydrocarbons at elevated temperatures on transition metal surfaces [65,66]. These results prove that dealkylation is sensitive to the processing environment, such as the catalysts composition, structure, and particle size. In line with this argument, Wang et al. showed that dealkylation and dehydrogenation reactions are related to the support's calcination temperature, which affects the interaction between the support and the metal ion distributed in it [67].

Understanding the mechanisms and analysing the catalytic activity for different materials are essential for efficient catalyst design. Jiang et al. compared the distribution of 12H-NEC dehydrogenation products for a series of noble catalysts on TiO_2 and found that the catalytic activity of noble metals is Pt > Pd > Rh > Au > Ru [68]. Fig. 5(e) shows the Pd/TiO_2 catalyst-based TEM image and Fig. 5(f) shows the hydrogen release during 12-NEC dehydrogenation on various noble catalysts at 180 °C in 420 min. The kinetics calculations show that the transition of 4H-NEC to NEC is the rate-determining step among all the dehydrogenation steps. However, the stability of TiO_2 in reducing hydrogen gas environment requires investigation in this case. If unstable, such catalysts might not be recyclable.

Wan et al. investigated the effects of hydrogen pressure, temperature, dosage, and stirring speed on the performance of Ru-based catalysts on NEC hydrogenation, as shown in Fig. 6 [69]. The hydrogen uptake rate increases with pressure, dosage, and stirring speed but saturates at 6–7 MPa, 1.0 g of catalyst, and 600 rpm, respectively. On the other hand, the hydrogen uptake rate reaches maximum in the range 95 °C–180 °C. It decreases at higher temperatures, probably due to the system's reduced catalytic activity and restricted hydrogen mass transfer. The reaction conditions and catalysts strongly influence the catalytic selectivity [58]. For hydrogenation of NEC, Pt, Ru, and Ni were found to be more suitable with temperatures of 120-230 °C and hydrogen pressure between 50 and 70 bar [39,70–76]. Similar to the dehydrogenation case, side reactions such as disproportionation, *N*-ethyl bond cleavage, and alkyl transfer are possible during the hydrogenation case, which may reduce the efficiency of the reaction [77]. Hence, strategies should be formulated in catalyst design to manipulate these side reactions [43], which significantly affect the system's performance.

3. Catalysts for NEC

Efficient catalysts are crucial for successfully implementing LOHC technology and should have the ability to achieve >80% hydrogenation/dehydrogenation of the hydrogen carrier under the following conditions (Temperature: <200 °C, pressure: <10 MPa). Also, a stable catalyst during the hydrogen storage cycle can have a significant economic impact. If the catalyst changes in phase during the hydrogen storage cycle, the new phase formed should be favourable for the process. During its functioning, catalysts are expected to have optimum binding to the reaction intermediates [78]. In the case of weak binding, the reactant's adsorption to the substrate is complex, resulting in low catalytic activity. On the other hand, strong binding limits the regeneration of catalytic surface sites. The binding depends on many factors, such as crystal structure, material, morphology, and particle size. For LOHC technology, the design of catalysts can be mainly focussed on accelerating low-temperature dehydrogenation to overcome the thermodynamic barrier, in view that compared to hydrogenation, endothermic dehydrogenation requires high heat [79]. For efficient large-scale NEC application, nano catalysts can be prepared through top-down approaches, such as ball milling, and bottom-up approaches, such as hydrothermal synthesis. However, it should be noted that before proceeding to large-scale applications, it is essential to test the hydrogenation reaction on a pilot scale using catalyst modules such as a fluidized bed since it is not practical to use suspended powder catalysts in large-scale applications [80]. A combination of techno-economic analysis (TEA) and life cycle assessment (LCA) should be conducted to understand the process of hydrogenation of NEC better before proceeding towards large-scale application. In the following sections, we discuss several vital catalysts for NEC studied to date, including ruthenium-, nickel-, palladium-, and platinum-based catalysts.

Table 1
Comparison of liquid organic hydrogen carriers [37,41,44–55].

System	Density (Kg/m^3)	Advantages	Challenges
● Hydrogen, ● Carbon, ● Oxygen, ● Nitrogen, ● Boron			
N-ethylcarbazole ($C_{14}H_{13}N$) 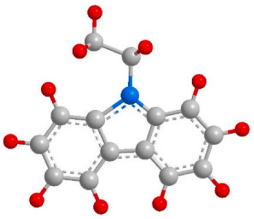	1059	• Ability to undergo hydrogen storage cycle under 200 °C [36] • Hydrogen storage capacity of 5.8 wt% [37] • Good structural stability, low reaction temperature, and high boiling point (348.3 °C) [38]	• High H_2 pressure required for the hydrogenation step with different catalyst required for both dehydrogenation and hydrogenation[39-41] • Hydrogen-lean form solid at room temperature [42] • Cracking of H12-NEC during dehydrogenation [43]
Phenazene ($C_{12}H_8N_2$) 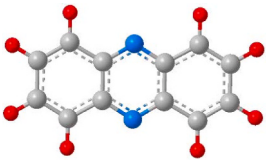	1250	• High storage capacity of 7.2 wt% [42] • Low dynamic viscosity an advantage for pumping LOHC [44] • Low vapor pressure results in simple storage [44]	• High toxicity potential indicator of 38.0 TPI/mg [44] • Solid at room temperature necessitating the addition of solvent. • Low flash point
Dibenzyl toluene ($C_{21}H_{20}$) 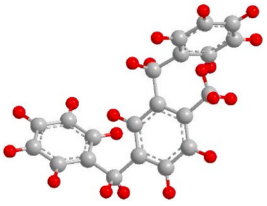	1029	• Gravimetric hydrogen storage capacity (6.2 wt%), high boiling point (380 °C), and low melting point (-90 °C) [8, 45] • Hydrogen-lean form H0-DBT is available as heat transfer oil since 1960 • Available in the form of the isomeric mixture at a relatively low cost (tradename e.g. Marlotherm SH, 2-4 €/kg on a ton scale)[46] • Well-investigated and benign ecotoxicological and toxicological properties along with excellent reversibility and favourable thermophysical properties [47-49]	• H18-DBT and H0-DBT have a viscosity of 389 mPa and 49 mPa, respectively, at 20°C, producing considerable impact on the pumpability of the system [46] • High temperature required for hydrogen discharge [46] • Slow diffusibility of all the involved dibenzyl toluene in the porous catalyst [46]

Toluene (C_7H_8) 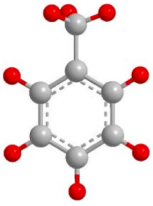	867	• High stability and low toxicity [44] • Liquid under ambient conditions. • No CO_2 emissions during the dehydrogenation process [50]	• Dehydrogenation takes place at a temperature between 250-450 ºC [44] • Flammable • Methylcyclohexane dangerous to the environment [44]. • Gaseous during the dehydrogenation process; a downstream hydrogen purification step is necessary [44]
Naphthalene ($C_{10}H_8$) 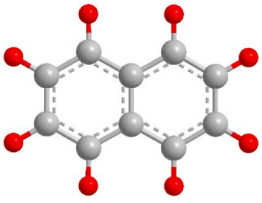	1140	• Storage capacity of 7.4 wt% [44] • Energy density of 2.2 kWh/L [44] • The high boiling points of naphthalene (218 ºC), cis-decalin (196 ºC), and transdecalin (187 ºC) make the evaporation loss negligible [51]	• Naphthalene has high melting point (80 ºC) [52] • Irreversible reaction of decalin to naphthalene [53] • Due to material properties, unsuitable for transportation and storage

1,2-dihydro-1,2-azaborine (C_4H_6BN) 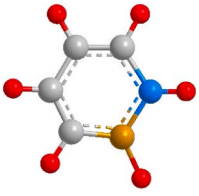	-	• Energy density of 2.4 kWh/L and high storage capacity of 7.1 wt% [44] • Low temperature dehydrogenation of 80 ºC, total yield at this temperature [54] • Low heat demand of 5.9 kJ/molH_2 during dehydrogenation [55]	• Solvent tetrahydrofuran must be added since, at ambient temperature, 1,2-BN-cyclohexane is not liquid. • Low flash point makes dehydrogenation difficult. • Reduction of storage capacity to 2-3 wt% after the addition of solvent

3.1. Ruthenium-based catalysts

Eblagon et al. performed a comprehensive experimental and theoretical investigation of Ru-catalysed hydrogenation [33]. They performed a hydrogenation reaction with an NEC/catalyst ratio of 20/1 in 100 mL cyclohexane as solvent and found that solvent cyclohexane increases the reaction rate but does not significantly change the conversion and selectivity, which are inversely correlated with the catalyst particle size. Their investigations show that a 5 wt% Ru/Al_2O_3 catalyst prepared under mild chemical reduction with many low coordination sites accelerates the conversion of intermediates to fully hydrogenated products. Computationally, they found that NEC prefers to adsorb at flat terrace sites. In contrast, the 8H-NEC intermediate prefers step sites due to their different steric features, and this preference is related to the shape of the hydrogenated products, as shown in Fig. 7.

Recently, Tang et al. also conducted comprehensive calculations on the dehydrogenation of H12-NEC on the Ru(0001) surface, examining various reaction pathways that span from H12-NEC adsorption to hydrogen release and NEC desorption, as shown in Fig. 8 [62]. Their work identified the desorption of NEC as the critical or most energy-demanding step. It also confirmed that dealkylation is possible at elevated temperatures. To capture the effects of surface complexity, Tang et al. extended their analysis to include an amorphous Ru phase. For 8H-NEC, they observed a stronger bond with the amorphous surface compared to the flat crystalline surface, aligning with Eblagon et al.'s findings that 8H-NEC prefers binding to step sites. In contrast, 4H-NEC and NEC exhibited weaker bonding to the amorphous surface, which may promote NEC desorption. The tendency of hydrogen-poor molecules (4H- and 0H-NEC) to bond weakly with amorphous surfaces is attributed to the enhanced interaction of planar aromatic rings with flatter crystalline surfaces (Fig. 8(b)).

Qin et al. [81] compared the performance of Ru/Al_2O_3, commercial Ru/C, $Ru/BC\text{-}NaBH_4$ (bio-carbon with $NaBH_4$ as a reducing agent), and RuNPs/pg-BC (Ru nanoparticles supported by partially graphitised bio-carbon). Ru/pg-BC performs best among the catalysts in conversion and 12H-NEC yield, as shown in Fig. 9(a-d). They attributed the excellent performance of Ru/pg-BC to the reluctant agglomeration of Ru NPs during the reaction cycles as they were trapped in the cavities of pg-BC formed during the carbothermal process. By investigating the effect of reaction condition on hydrogenation of NEC, Shi et al. showed that for Ru/Ni–Fe-layered double hydroxide (LDH) (catalyst), the 12H-NEC yield and NEC hydrogenation increased initially as pressure increased but remained unchanged when pressure condition was higher than 6 MPa [82].

Their investigation also revealed that as the temperature increased, the hydrogenation rate of NEC increased and then decreased slightly which they attributed to low solubility of hydrogen at high temperatures.

3.2. Nickel-based catalysts

Ye et al. studied the Raney-Ni catalyst for hydrogenation of NEC [71]. They investigated the effects of catalyst, pressure, and reaction temperature on mass transfer reaction processes, as seen in Fig. 10(a–c). The results showed that the reaction rate accelerates with increased temperature and becomes saturated at around 200 °C, following a similar trend to Ru-based catalysts, shown in Fig. 10 [69].

Liu et al. compared the performance of $0.1Rh–Ni/\gamma\text{-}Al_2O_3$ (0.1 wt% Rh) with monometallic $Ni/\gamma\text{-}Al_2O_3$ and 1 wt% $Rh/\gamma\text{-}Al_2O_3$ for the hydrogenation of NEC and found that the bimetallic catalyst achieved hydrogen storage capacity of 5.63% in 2 h [83]. The superior property of $0.1Rh–Ni/\gamma\text{-}Al_2O_3$ was attributed to the electron transfer and synergy effect between Ni NPs and Rh. The synergic effect results in smaller Ni NPs and better selectivity for 8H-NEC towards 12H-NEC (Fig. 10(f-g)). This result agrees with the computations by Eblagon et al. that 8H-NEC prefers step sites [33], which are more likely on smaller particles. It should be noted that investigating non-noble metals for creating step sites in catalysts has the potential to reduce cost, which requires investigation. Wu et al. demonstrated complete hydrogenation of NEC in 5.6 h by mixing Ni/Al_2O_3 with metal hydride YH_3 [84]. As shown in Fig. 10 (h), the atomic hydrogen in YH_3 can be transferred directly to the NEC molecule, resulting in hydrogen vacancies in YH_3, which are refilled through H_2 molecule adsorption into YH_3. Their performance is comparable to that of the best-performing Ru/Al_2O_3 catalysts. However, Ni/Al_2O_3 alone achieved hydrogen uptake of only 0.3 wt% over 8 h. Their investigation revealed Ni/Al_2O_3 is required to activate NEC molecules. Also, the hydrogenation efficiency of large Ni particles was higher than that of small particles (Fig. 10(i)). The reason for this is hydrogen adsorption depends on the YH_3–Ni interface, which is more readily available in the case of large Ni particles (Fig. 10(j)). Ding et al. studied the hydrogenation of NEC and other LOHCs using 70 wt% Ni catalysts supported by Al_2O_3, SiO_2, and Al_2O_3–SiO_2 [85]. The catalyst with equal molar Al and Si in its support exhibited excellent performance, better than commercial 0.5 wt% Ru/Al_2O_3. Their studies revealed that the agglomeration of Ni, which causes catalyst deactivation, can be inhibited by the strong interaction between Ni and Al_2O_3. Introducing SiO_2 in the support also helps reduce Ni. Wang et al. conducted NEC hydrogenation with different Ni/Co ratios and found an enhanced catalytic activity with increased cobalt content [86]. They found that catalyst activity is best when the Ni/Co ratio is 1, and the activity of the catalyst is affected by the metal electronic structure.

The nickel-based catalyst prevents the deposition of carbon on active nickel sites, which has resulted in good catalytic behaviour for the hydrogenation of NEC. Wang et al. investigated Ni/Al hydrotalcite oxides prepared using various Ni/Al ratios to support Ru NPs [87]. They found that Ni–Al interactions resulted in a difference in activity since these interactions resulted in lattice defects. The crystal defects resulted in small and dispersed Ru NPs since they enhanced the adsorption of Ru^{3+}, and the activity of Ru NPs increases as their size decreases.

3.3. Palladium based catalysts

Yang et al. compared the dehydrogenation activity of Pd with other common noble metals and found the activity was of the order Pd > Pt > Ru > Rh with Alumina as support [38]. For Pd and Pt, 100% conversion to NEC was achieved in 5 h at 180 °C and 1 atm, while for Ru and Rh catalysts, the fraction of NEC in the final products was 71.4% and 10.6%, respectively. By fitting the experimental data of the three-stage dehydrogenation (12H-NEC → 8H-NEC → 4H-NEC → NEC) into a first-order kinetic model, the authors found that, for all catalysts in the study, the reaction rate decreased substantially with time. Also, they proposed that reaction 4H-NEC → NEC is the rate-limiting step during the de-hydrogenation process, consistent with the computational findings of Tang et al. [78].

Later, Jiang et al. investigated the dehydrogenation activity of a series of noble metals (Pt, Pd, Ru, Rh, and Au) supported by SiO_2 [88]. They found the activity order to be Pd/SiO_2>Pt/SiO_2>$Rh/\text{-}SiO_2$>Ru/SiO_2>Au/SiO_2, which is similar to the findings of Yang et al. [38], except Rh has higher activity than Ru. Both experiments were conducted at the same reaction temperature (180 °C) but with different supports, which provides the case for investigating the role of supports during the hydrogenation process. Also, the stability of SiO_2 in reaction conditions of dehydrogenation requires investigation.

Wang et al. investigated dehydrogenation of 12H-NEC on the plane (100), (110), and (111) of Pd nanoparticles supported on rGO [89] and found the catalytic efficiency follows the order Pd(111) < Pd(110) < Pd (100). This is understandable since the density of surface electrons, which depends on the surface atomic structure, also increases in that order. Jiang et al. investigated bimetallic $Pd–Au/SiO_2$ catalysts prepared by incipient wetness of silica gel [88]. They confirmed a positive correlation between Au amount and particle size and the lack of alloy structure in the catalysts proposed through XPS analysis. Their

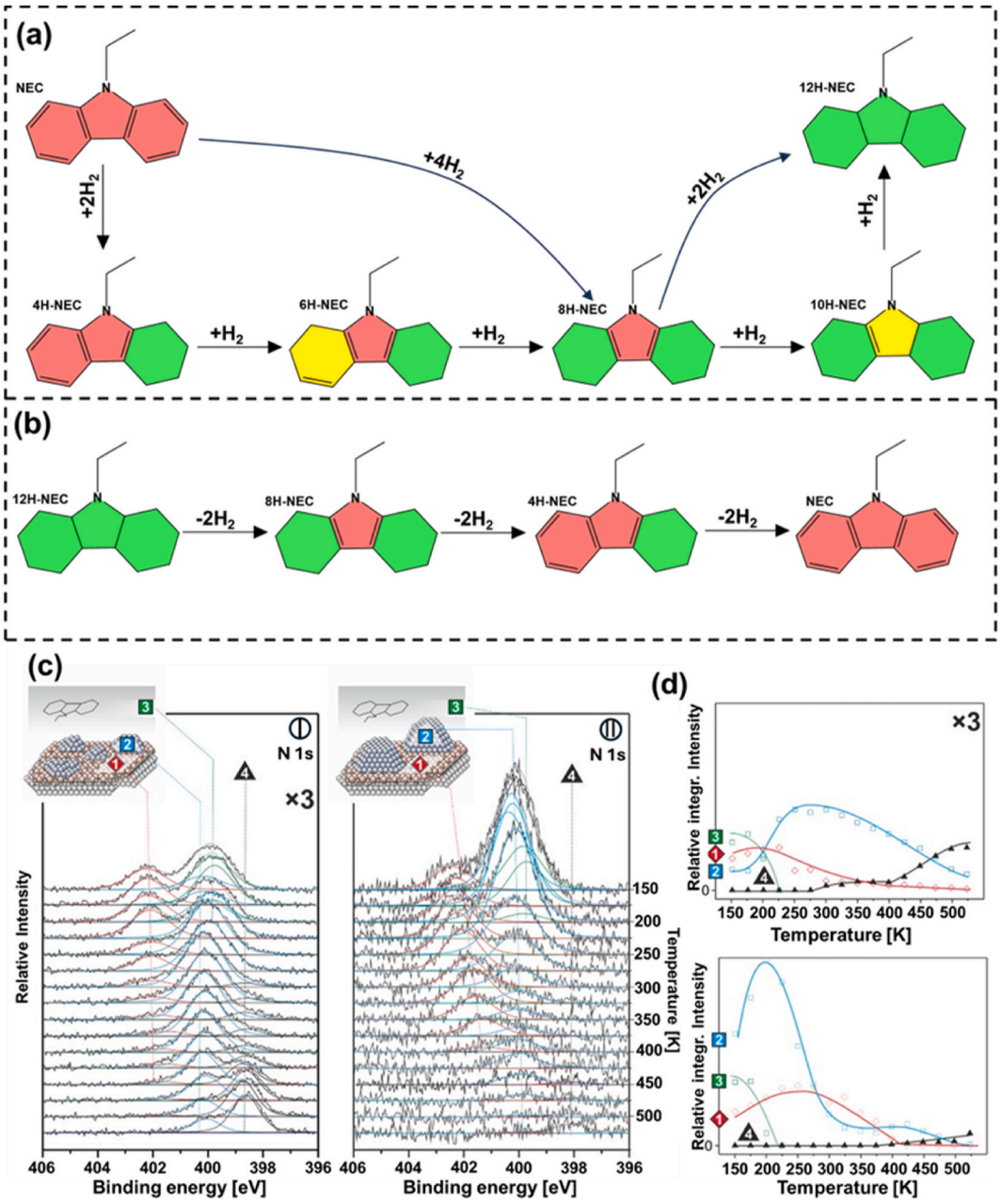

Fig. 4. The overall mechanism of hydrogen storage in NEC, (a) hydrogenation and (b) dehydrogenation (red shows an unsaturated ring, yellow shows a partially saturated and green shows a fully saturated ring). (c) Thermal evolution of N 1s region for 12H-NEC on small Pt aggregates (left) and ordered Pt nanocrystallites (right), with the support of Al_2O_3/NiAl(110). (d) quantitative analysis of the N 1s peaks as a function of temperature [43] Peak 1: Al_2O_3 adsorbed 12H-NEC, peak 2: chemisorbed NEC on Pt, peak 3: 12H-NEC multilayer physisorbed, and peak 4: dealkylated 12H-NEC. Reprinted (adapted) with permission from Ref. [43]. Copyright (2014), American Chemical Society. (For interpretation of the references to colour in this figure legend, the reader is referred to the Web version of this article.)

investigation found a negative correlation between particle size and dehydrogenation activity. The activity order was Pd_3Au > PdAu > Pd > $PdAu_3$. They claimed that the binding of all intermediates to PdAu(111) is stronger than to Pd(111), based on first principles calculations. Like hydrogenation, the increased concentration of step sites in smaller particles may also play a role during dehydrogenation, requiring investigation. Later, the authors extended their studies to other bimetallic catalysts Pd-M/SiO_2 (M = Cu, Ni) and reported the performance order of Pd_3M > PdM > Pd > PdM_3>M, with Pd_3Ni showing the highest performance of 100% conversion, 91.1% selectivity of NEC and 5.63 wt % hydrogen release at 180 °C, 1 atm for 8 h [90]. They attributed the enhanced performance of alloyed Pd to its modified electronic structures and the decreased performance upon over-alloying to the active site blockage by excessive M. Other research groups supported the above findings. For example, Wang et al. checked a series of Pd–Cu catalysts supported by reduced graphene oxide [91] for the dehydrogenation process. They found that excellent performance of pure Pd was maintained when the content of Cu was below 50%, but further addition of Cu resulted in electron transfer from Pd to Cu, resulting in reduced dehydrogenation activity.

Shuang et al. studied the impact of Pd oxidation states on its catalytic performance [92]. They compared the dehydrogenation of a hydrogenated LOHC mixture (40 wt% 2-methylindole, 36 wt% N-propyl carbazole, and 24 wt% NEC) catalysed by Pd/AC and PdO/AC. They observed significantly higher yield and conversion for PdO/AC under mild conditions, with 100% conversion and 98.5% yield at 100 °C for 60

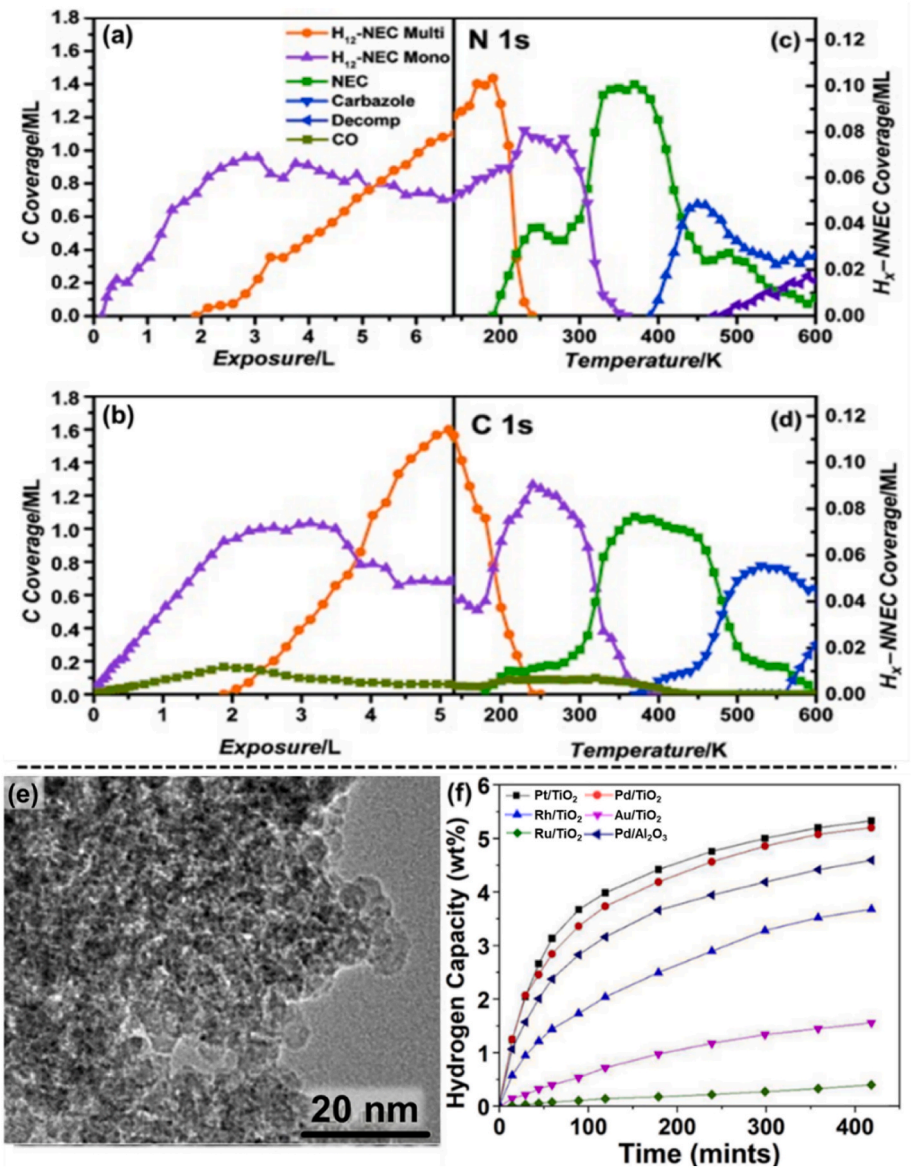

Fig. 5. The quantitative analysis of XPS spectra of 12H-NEC upon its adsorption and reaction on Pt(111) [63]. The absorption and reaction of (a, c) N1s and (b, d) C1s respectively, reprinted with permission from Ref. [63]. (e) TEM image of Pd/TiO_2 catalyst, (f) 12H-NEC dehydrogenation on various catalysts in 420min at 179.85 °C. Reprinted (adapted) with permission from Ref. [68].

h and full hydrogen release at 140 °C for 8h. The authors found that oxidation cleaned the components that block the pores of Pd/AC, resulting in dramatically higher surface area, micropore area, and micropore volume, and, therefore, new active sites for better catalytic activity. However, it should be noted that the stability of PdO in a highly reducing hydrogen gas atmosphere at reaction temperature requires investigation. It should also be noted that PdO may convert back to Pd during dehydrogenation. In-situ experiments in cases like this can provide insight into the catalyst mechanism and its role in the hydrogenation process.

The effects of supports on Pd catalyst performance were also studied. For example, Wang et al. found that compared to Pd/Al_2O_3, Pd catalysts supported by reduced graphene oxide (rGO) have smaller Pd particles with more active sites and better dehydrogenation performance [93]. Zhu et al. synthesised Pd supported on carbon nanotubes and found their 3 wt% Pd/CNT resulted in 5.8 wt% hydrogen produced at 260 °C with a conversion of 99.6% [94]. Li et al. found that introducing Co into Pd could achieve high levels of dehydrogenation at a relatively low temperature due to the changes in the electronic state, the interfacial effect of Pd, and the interaction with defects in support [95].

3.4. Platinum-based catalysts

Gong et al. investigated the effect of Pt loading on the dehydrogenation efficiency of Pt/TiO_2 catalysts [96]. They found that optimum performance occurs at 1 wt% of Pt on TiO_2 support, and lower Pt loading results in a decrease in performance due to reduced active sites. Increasing the Pt amount did not increase catalytic activity. They attributed this to the Sabatier principle, where too strong or too weak interaction might limit the reaction rate. The Pt nanoparticles supported on TiO_2 were considered an electron-rich state, confirmed by the negative direction shift of $Pt^0 4f_{7/2}$ in the XPS analysis when Pt-loading on TiO_2 increased from 0.5 wt% to 1 wt%. The excellent performance was attributed to the strong metal-support interaction (SMSI) accelerating the rate-limiting step. The authors claim better selectivity, activity, and stability of their Pt-based catalysts for 12H-NEC dehydrogenation than the 5 wt% commercial Pd/Al_2O_3 catalyst. Peters et al. investigated the impact of mass transfer on the dehydrogenation of 12H-NEC by

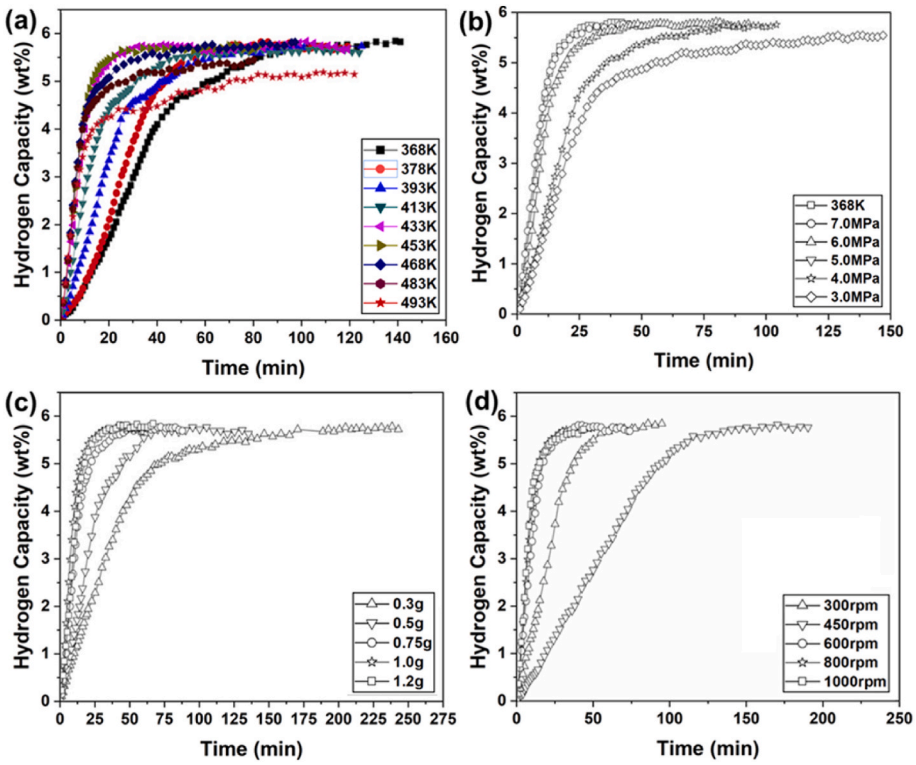

Fig. 6. The effect of various parameters on the hydrogenation of NEC with Ru-based catalysts. (a) temperature, (b) pressure, (c) dosage of catalyst, and (d) stirring speed. Reprinted from Ref. [69].

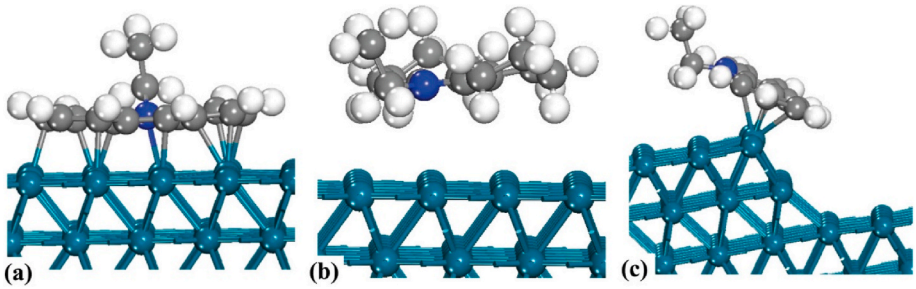

Fig. 7. (a) Terrace sites of Ru (001) with NEC adsorbed on it. (b) 8H-NEC intermediate desorption in the energetically favourable way on Ru(001), (c) Stepped Ru (109) with two atomic heights with NEC adsorbed on it. The energies are E(a) = 2.56 eV E(b) = 0.32 eV, E(c) = 1.61 eV [33]. Reprinted (adapted) with permission from Ref. [33].

coating an active, porous γ-alumina shell layer of various thicknesses, impregnated with platinum, on a non-porous α-alumina core [97]. In the temperature range investigated (224–261 °C), the authors highlighted the role of pore diffusion on the productivity of precious metals. Even for layers as thin as 24 μm, the kinetic regime is limited to 235 °C. 12H-NEC needs to diffuse through the porous layer to react with Pt atoms, resulting in decreased activity per metal due to the layer being thicker than the mean diffusion length of the molecule. In such a scenario, Pt atoms get underutilised since 12H-NEC reacts before reaching them, reducing the overall activity of Pt. This experiment illustrates that catalyst structure and conditions should be considered to obtain an efficient dehydrogenation reaction.

Tarasov et al. found that introducing a second metal (Cr, Pd) enhances Pt/Al_2O_3 catalyst activity for 12H-NEC dehydrogenation [98]. Investigation revealed that Cr addition affects Pt's electronic state and local environment, with the average Pt nanoparticle size in $Pt–Cr/Al_2O_3$ about two times smaller than Pt/Al_2O_3. The results show the importance of catalyst surface structure in the hydrogenation/dehydrogenation cycle. Similarly, Li et al. employed $Ti_3C_2T_x$ with a series of catalysts for studying the catalytic activity, stability, and selectivity for dehydrogenation of 12H-NEC [99]. They found that 3 wt% $Pt/S–Ti_3C_2T_x$ achieved 5.62 wt% hydrogen release, 91.55% selectivity of NEC and 100% conversion. Enhanced performance is attributed to a large area and strong interaction, especially electron transfer between $S–Ti_3C_2T_x$ and Pt. Alberto et al. investigated Ni nanoparticles anchored on an N-doped graphitic carbon matrix [Ni@(N)C] as the hydrogen storage/release catalyst on *N*- ethylcarbazole. They found that adding a minute amount of Pt (18 ppm) increased the catalytic activity of Ni@(N)C due to H spillover to the Ni NPs promoted by Pt. There was no linear correlation between the catalyst activity and Pt concentration. They attribute this result to single atoms or small Pt clusters at lower concentrations than large, less efficient cluster regimes resulting from higher concentrations [100]. These results again point out the role of defects in the functioning of the catalyst for the NEC hydrogen storage cycle. Investigating whether a similar effect can be achieved by designing non-noble metals to create defects could pave the way for efficient catalysts in the future.

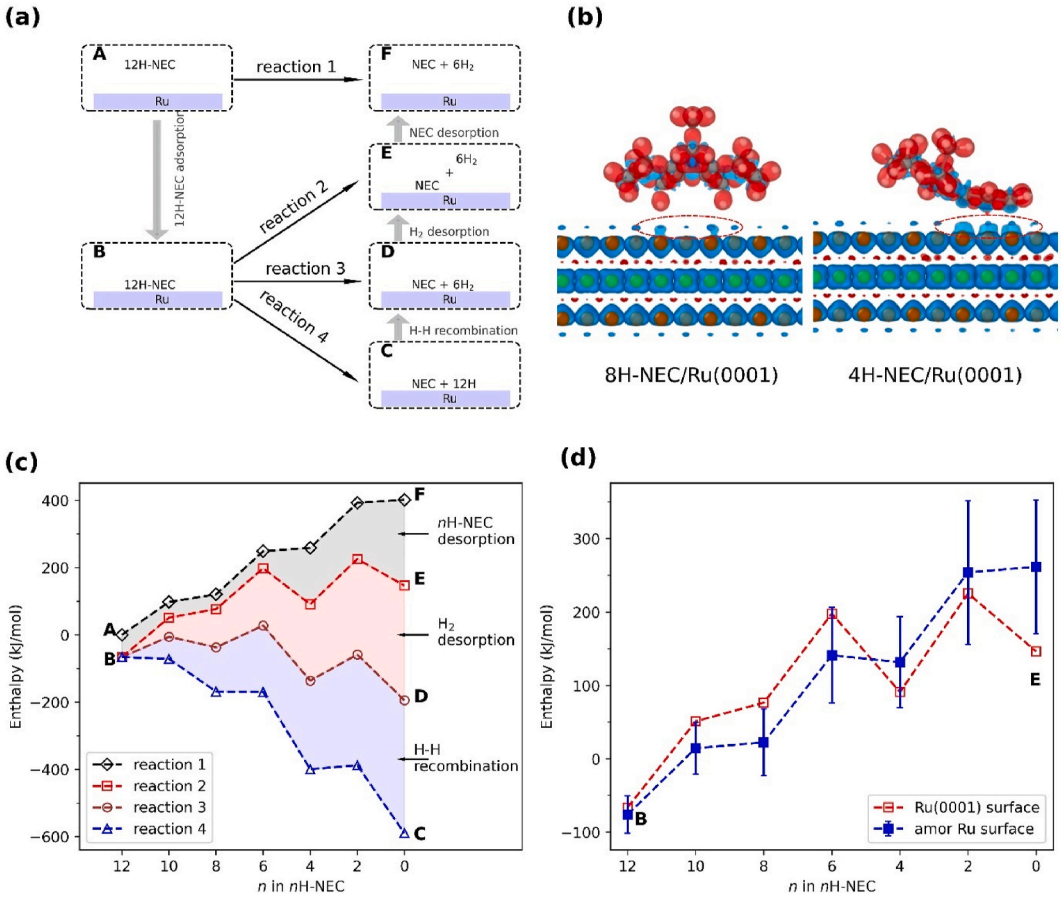

Fig. 8. Computational dehydrogenation of 12H-NEC on Ru surface. (a) Schematic of the process, (b) Isosurface of differential charge density showing stronger bonding of the flat aromatic ring of 4H-NEC to flat Ru surface, (c) Relative system energy as a function of dehydrogenation step and reaction route. Energy kinks at n = 8 and 4 indicate 8H-NEC and 4H-NEC are stable intermediates, (d) Reaction 2 on crystalline and amorphous Ru surfaces. Replotted from Ref. [62].

4. Support for catalysts

Ideally, catalyst support should have a high surface area for maximum dispersion of active sites, optimum porosity to facilitate the diffusion of reactants and products, mechanical strength to withstand reaction conditions, thermal stability to withstand operating conditions temperature, and chemical stability that resists change in reaction conditions. In case of (de)hydrogenation of LOHCs, the impact of catalyst support has been widely observed [74,101,102].

Eblagon et al. studied the hydrogenation of molten NEC using catalysts Ru, Pd, Pt, and Ni on various supports (Table 2) [39]. For Ru, the catalytic activity for different supports is in the order Al_2O_3 >TiO_2 > SiO_2–Al_2O_3 > zeolite > graphite > Activated carbon (AC). Their investigation revealed that hydrophilic support in hydrogenation could produce kinetically favoured but thermodynamically less stable *cis*-isomer of 12H-NEC [74], which is desirable for easier dehydrogenation. For dehydrogenation of 12H-NEC by Pd nanoparticles on different supports, Feng et al. found the activity order to be Pd/AC > Pd/Al_2O_3 > Pd/TiO_2 > Pd/SiO_2 [103]. The results are similar to the study of Ru by Eblagon et al. [39], except that Ru supported by activated carbon has the lowest activity. The authors attributed the high activity of Pd/AC to the large surface area and pore volume (1754 m^2/g and 1.533 cm^3/g). However, in the case of Ru, the surface area of Ru/AC is the highest, but the performance was not the highest among compared catalysts (Table 2). These results show that the material selection and its design might play a significant role during dehydrogenation rather than only the surface area of the catalyst.

Wu et al. studied NEC hydrogenation using Ru/YH_3 and Ru/Al_2O_3 catalysts at 403 K and 7 MPa and observed superior activity for Ru/YH_3 [104]. The surface area of Ru/Al_2O_3 was larger than Ru/YH_3, and the electronic effects of support materials were the same on both Ru/Al_2O_3 and Ru/YH_3, confirmed by XPS. The sizes of Ru were also similar in both cases. They found that the leading products on Ru/YH_3 are all-cis products that can be dehydrogenated with less steric hindrance. The enhanced activity was also found with other rare earth hydride supports, such as LaH_3 and GdH_3. The enhanced activity results from the different hydrogen transfer paths through the metal hydride [84], as discussed in Fig. 10(h-j). A similar phenomenon was also observed in the catalyst Pd/Al_2O_3 mixed with YH_3 [105]. These observations may be crucial since the design of cheaper metal hydrides as support for catalysts may provide a breakthrough for implementing this technology.

Yu et al. investigated the effect of different TiO_2 supports on bimetallic Ru–Ni catalysts [106]. Adding Ni to Ru improves the hydrogenation performance in the cases of P25 and anatase TiO_2 support. However, it deteriorates the performance of rutile TiO_2 support, as shown in Fig. 11(a-b). For anatase support, the promotion effect of Ni was attributed to an intra-particle hydrogen spillover effect, while the deterioration in the rutile case was attributed to severe metal aggregation. For both Ru and Ru–Ni, P25 support offers the best performance, which was attributed to some synergetic effect because of the lower specific surface area of Ru/P25 compared to Ru/Anatase. Fig. 11(a-b) shows that the impact of support is also dependent on catalyst material.

5. Bidirectional catalyst

In practice, there exist scenarios where it would be desirable for hydrogenation and dehydrogenation to occur in the same reactor, and the presence of two types of catalyst increases the system's complexity

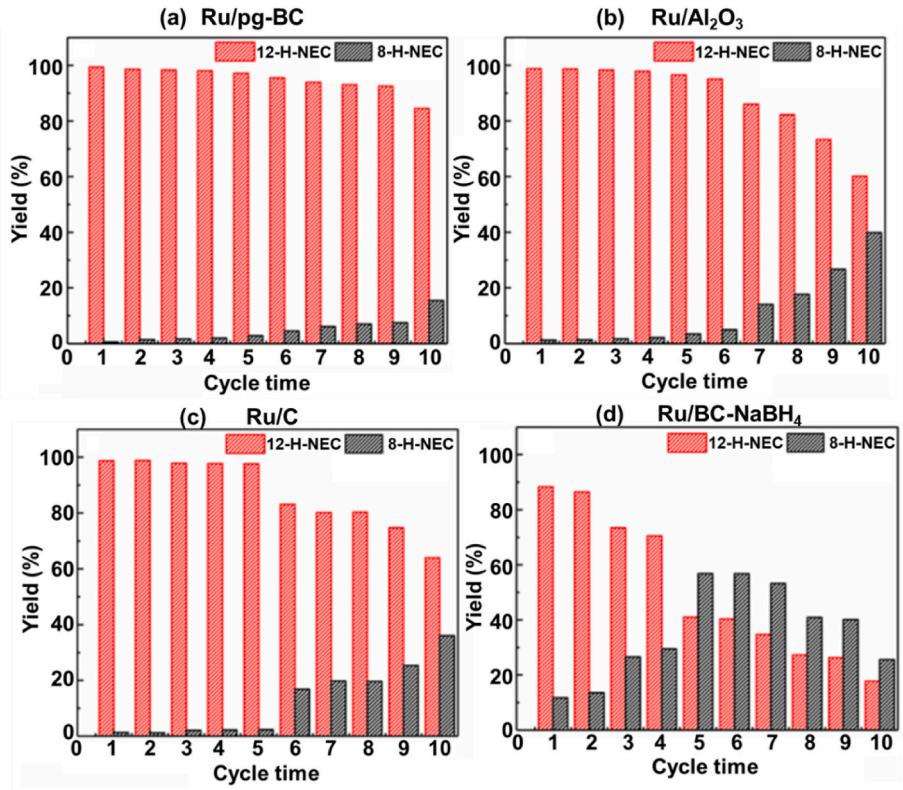

Fig. 9. Stability and performance of various catalysts during hydrogenation of NEC. (a) Ru/pg -BC, (b) commercial Ru/Al_2O_3, (c) commercial Ru/C, and (d) Ru/BC-$NaBH_4$. Reproduced with permission [81].

and cost. In this situation, bidirectional catalysts that allow both hydrogenation and dehydrogenation are desirable, and many groups have focused their efforts on this. Yu et al. developed a submicron $LaNi_{5.5}$ bidirectional catalyst of a unique core-shell structure with excessive Ni on the surface [107]. Hydrogen discharge during the reversible (de) hydrogenation reaction is impacted by the concentration of atomic hydrogen in the H–$LaNi_{5.5}$ solid solution and, in turn, the pressure of H_2 (Fig. 11 c-e).

A reversible hydrogen storage capacity above 5.5 wt% was achieved below 473 K for 9 cycles using 10 wt% $LaNi_{5.5}$, with a dehydrogenation performance similar to noble metal catalysts. Similarly, Yang et al. noticed that adding metal hydride YH_3 to Pd/Al_2O_3, a bidirectional catalyst, improves hydrogenation and dehydrogenation performance [105]. In addition to metal hydrides, combining two distinct catalysts is promising for developing bidirectional catalysts. Xue et al. [108] reported boosted cyclic (de)hydrogenation using bimetallic Pd–Rh nanoparticles supported by Al_2O_3, with hydrogen uptake of 5.43 wt% in 1 h and hydrogen release of 5.48 wt% in 4h. To understand the mechanism for the performance boost, the authors performed first-principles calculations of the enthalpy change for hydrogenation on Pd_6, Pd_4Rh_2, and Rh_6, all supported by γ-Al_2O_3(110). They found that for the reaction on catalyst Pd, each step is endothermic, with the total enthalpy change to be ~3.9 eV, while on catalyst Rh, each step is exothermic and adds up to ~ -2.5 eV for the whole reaction. Their investigation found a moderate enthalpy change (~-0.36 eV) for the reaction on Pd_4Rh_2, which favours reversible (de)hydrogenation. Forberg et al. developed a binary bidirectional catalyst, Pd_2Ru supported by SiCN [42]. They reported hydrogen uptake of 5.68 wt% (110 °C, 0.52 mol% active metal, 1 mmol NEC, 36 h, $p(H_2) = 20$ bar) and hydrogen release of 5.51 wt% (180 °C, 0.52 mol% active metal, 2 mmol 12H-NEC, 7h). Combining two metals increased efficiency (especially for dehydrogenation), resulted in high specific surface area, and reduced catalyst loading compared to Pd/SiCN.

Xue et al. investigated the bidirectional catalyst RhCo and found that the structure maximised Rh utilisation, boosting NEC's reversible (de) hydrogenation [109]. They realized complete hydrogenation at low temperature of 90 °C and found that adding Co resulted in the shift of the *d* band centre to the fermi level, as seen in Fig. 12. Adding Co improved catalytic activity by enhancing the adsorption of the reaction substrate on the catalyst.

6. Summary and outlook

In this review, we have provided a comprehensive account of the recent development of catalysts for NEC as a hydrogen carrier, focusing on various noble catalysts, support materials, and bidirectional catalysts. While recent years have seen massive research efforts and development in this field, large-scale NEC applications for hydrogen storage are still challenging given, for example, the stability, abundance, and cost of catalysts. Also, for LOHCs, a deep microscopic understanding of the catalytic process (such as the role of support materials) is still lacking, which hampers further development of efficient catalysts. These aspects need to be addressed to develop efficient catalysts. Specifically, we propose the future research directions listed in the following sections.

6.1. Low-cost catalysts

Currently, noble metals are the best-performing catalysts for the LOHC system. However, large-scale applications of noble catalysts for hydrogen storage are not practical because of their cost and availability. Either the content of the noble metals must be drastically reduced via, for example, single-atom catalysts (SACs), or new non-noble catalysts, such as transition metal oxides, must be developed. SACs contain individual isolated atoms which are coordinated or dispersed on support, optimizing the efficiency of metal atoms and reducing the cost [110].

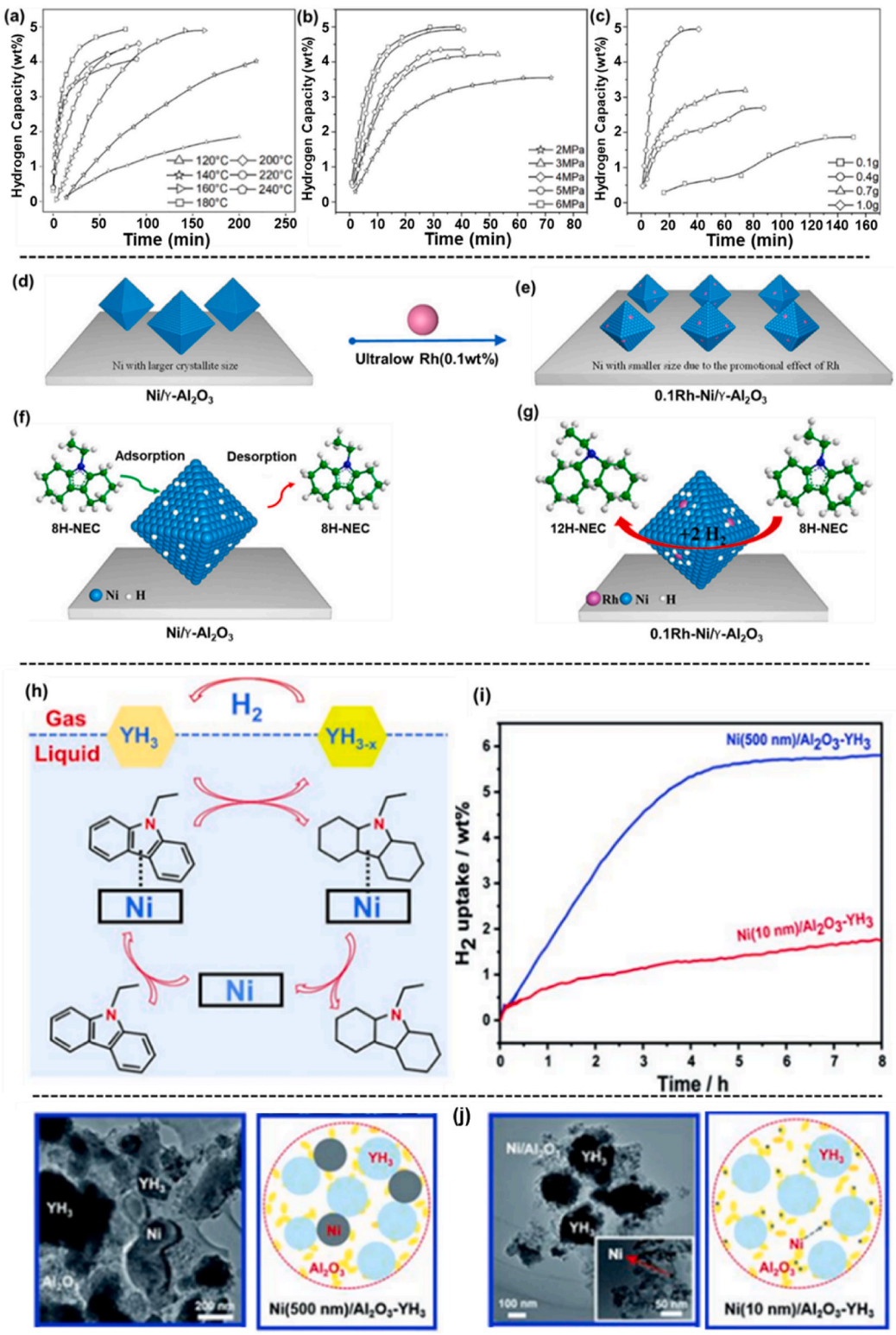

Fig. 10. (a–c) Hydrogenation of NEC under different conditions. (a) Temperature varied over 10 wt% Raney-Ni at 5.0 MPa, (b) Pressure varied over 10 wt% Raney-Ni at 200 °C, (c) Different weight % of catalyst at 5.0 MPa and 200 °C. Reprinted with permission [71]. (d–g) Schematic representation of hydrogenation of 8H-NEC to 12H-NEC on Ni/γ-Al_2O_3 and 0.1Rh–Ni/γ-Al_2O_3. Reprinted with permission [83]. (h–j) Synergetic hydrogenation of NEC on Ni and metal hydride YH_3 [84]. (h) Mechanism for synergetic hydrogenation of NEC catalysed by Ni/Al_2O_3-YH_3. (i) Effect of Ni particle size on NEC hydrogenation on Ni/Al_2O_3-YH_3 (150 °C, 3 MPa H_2, 1 g NEC, 25 mg Ni/Al_2O_3, and 100 mg YH_3). (j) TEM images and schematic illustrations of the catalysts. Reprinted with permission [84].

Table 2
Activity and selectivity of various catalyst/support for hydrogenation of NEC. The activity represents the amount of NEC converted per gram of metal per second (μmol/g/s), and the selectivity is for all 12H-NEC stereoisomers (%) at 130 °C and 70 bar (top panel). For dehydrogenation of 12H-NEC at 180 °C (bottom last 4 panels), the activity is in unit mol $_{NEC}$/mol $_{Pd}$/min, and the selectivity is for NEC. Metal particle diameter D_m, surface area A, pore diameter D_p, and specific pore volume Vp are averaged. COM stands for Commercial catalyst, whereas CR stands for chemically reduced. The chemical reduction method was carried out by drop-casting metal chloride salt solution onto a slurry of support and reducing using a solution of sodium borohydride.

Sample	Catalyst type	Activity	Selectivity	D_m (nm)	A (m^2/g)	D_p (nm)	V_p (cm^3/g)	Ref.
5 wt% Ru/Al_2O_3	CR	8.2	98	1.61	152	11.7	–	[39]
5 wt% Ru/Al_2O_3	COM	7.8	92	9.08	83	12	–	[39]
5 wt% Ru/SiO_2–Al_2O_3	CR	7.5	96	2.37	483	5.4	–	[39]
65 wt% Ni/SiO_2–Al_2O_3	COM	0.3	93	7.50	95	10.0	–	[39]
5 wt% Ru/zeolite	CR	7.2	78	2.31	343	3.2	–	[39]
5 wt% Ru/graphite	CR	7.2	64	2.30	7	35.3	–	[39]
5 wt% Ru/TiO_2	CR	7.9	96	2.11	191	14.6	–	[39]
5 wt% Ru/AC	CR	6.8	53	2.99	538	5.2	–	[39]
Ru black	COM	0.4	77	Aggregated	22	24.4	–	[39]
5 wt% Pd/AC	CR	1.5	2	–	–	–	–	[39]
65 wt% Ni/AC	CR	0.05	33	–	–	–	–	[39]
5 wt% Pt/AC	CR	0.1	0.6	–	–	–	–	[39]
5 wt% Pd/AC	COM	2.76	35.5	3	1754	–	1.533	[103]
5 wt% Pd/Al_2O_3	COM	2.50	56.9	4.7	190	–	0.509	[103]
5 wt% Pd/TiO_2	COM	1.97	35.9	1.7	57	–	0.334	[103]
5 wt% Pd/SiO_2	COM	0.30	20.2	Aggregated	160	–	1.592	[103]

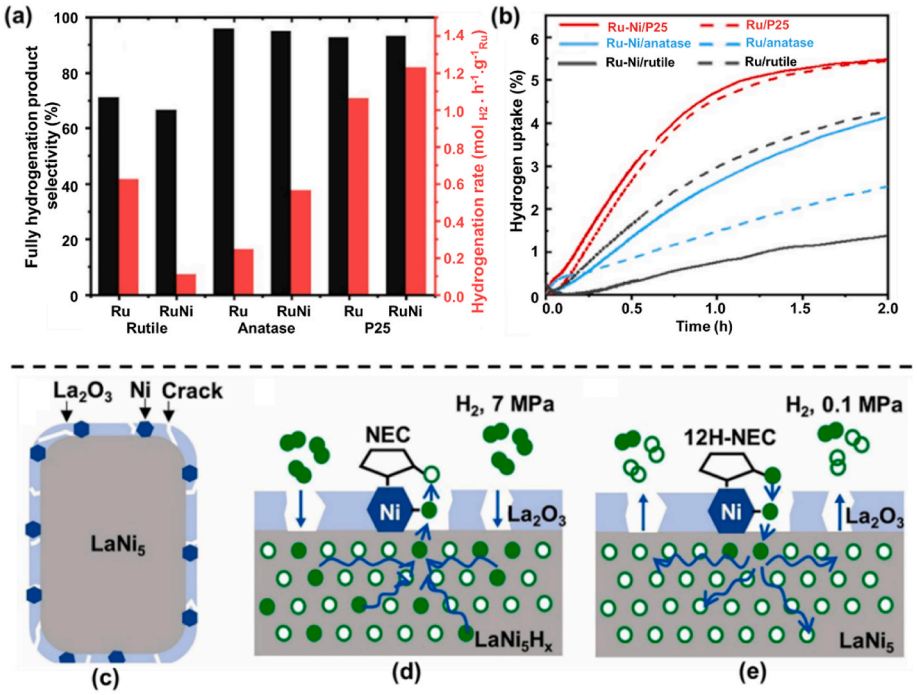

Fig. 11. (a) Performance of Ru and Ru–Ni catalysts with Rutile, Anatase, and P25 supports for selectivity and hydrogenation rate at 150 °C and 70 bar for 24 h (b) Hydrogen uptake for different catalysts in the first 2 h. Reproduced with permission [106]. (c) Structure of $LaNi_{5.5}$ nanoparticle. Transfer of hydrogen in $LaNi_{5.5}$ during (d) NEC hydrogenation (e) 12H-NEC dehydrogenation. Reproduced with permission [107].

However, the most common problem associated with SACs is the tendency to form aggregates due to the high energies of single metal atoms on the surface. Studies have shown that even though agglomeration takes place at high temperatures, the catalytic performance can be retained, proving that single atom catalyst can be used as low-cost catalysts [111]. SAC designed for (de)-hydrogenation of NEC can contribute towards development of low-cost catalysts. Metal-organic frameworks (MOFs) are another class of materials whose stability and efficiency for the hydrogenation process are worthy of investigation [112].

6.2. *Catalyst stability*

The research activities reviewed in this paper are mainly for laboratory scale, and for industrial applications, the stability of catalysts is an essential factor of concern and needs more investigation. For example, many experiments have shown that small catalyst particles dispersed on supports have good activity, but particle aggregation might occur during industrial applications due to temperature fluctuations and long-time operation. In addition to this, the recyclability data, which includes changes in the structure of catalyst during the hydrogen storage

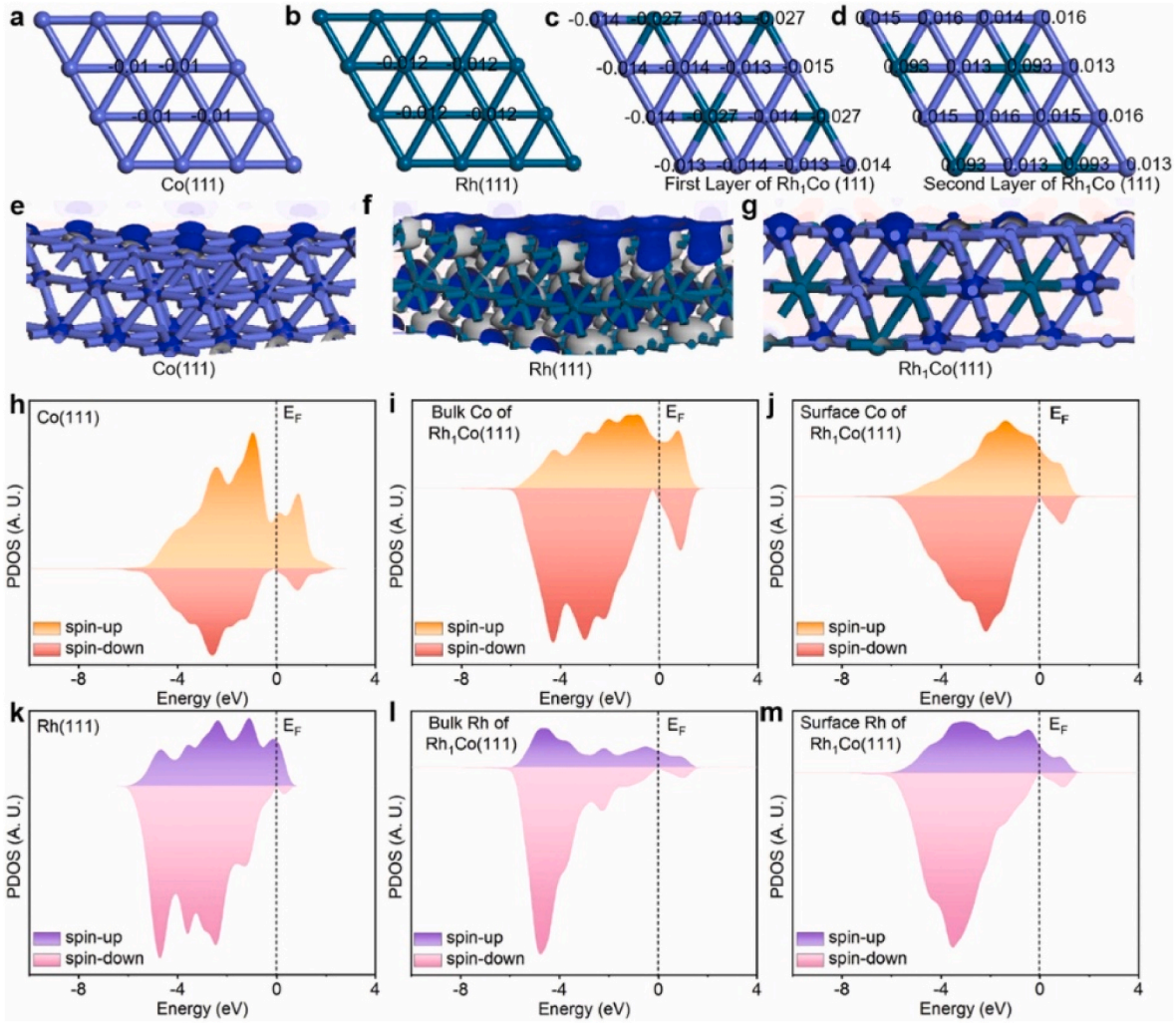

Fig. 12. Mulliken charge distribution of Co(111), Rh(111) and $Rh_1Co(111)$ (e–g) Charge distribution on Co(111), Rh (111) and Rh1Co(111) respectively (h–m) PDOS for the surface atoms of $Rh_1Co(111)$, Rh (111) and Co(111) Reproduced with permission [109].

cycle, are limited. A stable catalyst for multiple cycles has enormous economic implications, potentially making it competitive with other technologies. It should also be noted that there is a research gap in using oxides, including mixed metal oxides, as catalysts for the hydrogenation of NEC. The stability of these catalysts requires investigation. If any class of oxides is found to be unstable, new rules for catalyst design with the limited role of oxygen in the hydrogenation process are opened. The design of stable, efficient oxides that do not get poisoned during the hydrogenation process can make LOHC challenge other technologies cost-wise.

6.3. *CatalystSupport*

Support materials impact on the performance of catalysts for (de) hydrogenation, but this is a complex problem because of the number of combinations of catalysts and supports and the discrepancy in the literature. In addition, the mechanisms for catalyst-support interactions are to be understood systematically.

6.4. *Metal hydrides in the catalysts*

Recent investigations revealed a boost in catalyst performance resulting from introducing metal hydrides, which serve as an atomic hydrogen reservoir and provide new pathways for interacting NEC with hydrogen. The mechanism behind these new findings is yet to be understood, and more work can be done to engineer the hydrides, such as composition, structure, and distribution, for better performance.

CRediT authorship contribution statement

Preetham Permude: Writing – review & editing, Writing – original draft, Visualization, Validation, Methodology, Investigation, Formal analysis, Data curation, Conceptualization. **Chunguang Tang:** Writing – review & editing, Writing – original draft, Validation, Supervision, Methodology, Investigation, Conceptualization. **Adnan Ahmad:** Writing – review & editing, Visualization. **Hua Chen:** Writing – review & editing. **Terry Frankcombe:** Writing – review & editing, Validation, Supervision, Project administration, Funding acquisition, Formal analysis. **Yun Liu:** Writing – review & editing, Writing – original draft, Validation, Supervision, Project administration, Investigation, Formal analysis, Conceptualization.

Search strategy

The databases used are Google Scholar, PubMed, and Web of Science. The following search terms have been used for extracting articles: hydrogenation, *N*-ethylcarbazole, noble metals, noble metal free, catalyst, metal oxide catalyst, and hydrogen storage. The year range used is 1970–2024. Inclusion criteria: hydrogenation of *N*-ethylcarbazole using commercial or synthesised catalysts. Exclusion criteria: hydrogenation

of other LOHCs excluding *N*- ethylcarbazole using commercial or synthesised catalysts.

Declaration of competing interest

The authors declare the following financial interests/personal relationships which may be considered as potential competing interests: Yun Liu reports financial support was provided by Australian Research Council. Yun Liu reports financial support was provided by Australian National University. If there are other authors, they declare that they have no known competing financial interests or personal relationships that could have appeared to influence the work reported in this paper.

Acknowledgements

The authors would also like to thank Australian Research Council (ARC) for the linkage grant LP2000200472 through the Australian National University. The authors acknowledge the support from the Australian National University's grand challenge program Zero Carbon Energy for the Asia-Pacific (ZCEAP). The authors also acknowledge the feedback provided by Farzin Nekouei in the initial stage of manuscript.

References

[1] Züttel A. Hydrogen storage methods. Naturwissenschaften 2004;91:157–72. https://doi.org/10.1007/s00114-004-0516-x.
[2] Veziro T, Barbir F. Hydrogen: the wonder fuel. Int J Hydrogen Energy 1992;17:391–404. https://doi.org/10.1016/0360-3199(92)90183-W.
[3] Ulmer U, Hu J, Franzreb M, Fichtner M. Preparation, scale-up and testing of nanoscale, doped amide systems for hydrogen storage. Int J Hydrogen Energy 2013;38:1439–49. https://doi.org/10.1016/j.ijhydene.2012.10.115.
[4] Abdin Z, Tang C, Liu Y, Catchpole K. Large-scale stationary hydrogen storage via liquid organic hydrogen carriers. iScience 2021;24:102966. https://doi.org/10.1016/j.isci.2021.102966.
[5] Makepeace JW, He T, Weidenthaler C, Jensen TR, Chang F, Vegge T, Ngene P, Kojima Y, de Jongh PE, Chen P. Reversible ammonia-based and liquid organic hydrogen carriers for high-density hydrogen storage: recent progress. Int J Hydrogen Energy 2019;44:7746–67. https://doi.org/10.1016/j.ijhydene.2019.01.144.
[6] Usman MR. Hydrogen storage methods: review and current status. Renew Sustain Energy Rev 2022;167:112743. https://doi.org/10.1016/j.rser.2022.112743.
[7] Markiewicz M, Zhang Y, Bösmann A, Brückner N, Thöming J, Wasserscheid P, Stolte S. Environmental and health impact assessment of Liquid Organic Hydrogen Carrier (LOHC) systems–challenges and preliminary results. Energy Environ Sci 2015;8:1035–45. https://doi.org/10.1039/C4EE03528C.
[8] Teichmann D, Arlt W, Wasserscheid P. Liquid Organic Hydrogen Carriers as an efficient vector for the transport and storage of renewable energy. Int J Hydrogen Energy 2012;37:18118–32. https://doi.org/10.1016/j.ijhydene.2012.08.066.
[9] Bae J-E, Wilailak S, Yang J-H, Yun D-Y, Zahid U, Lee C-J. Multi-objective optimization of hydrogen liquefaction process integrated with liquefied natural gas system. Energy Convers Manag 2021;231:113835. https://doi.org/10.1016/j.enconman.2021.113835.
[10] Akhtar MS, Dickson R, Liu JJ. Life cycle assessment of inland green hydrogen supply chain networks with current challenges and future prospects. ACS Sustainable Chem Eng 2021;9:17152–63. https://doi.org/10.1021/acssuschemeng.1c06769.
[11] Dwivedi SK, Vishwakarma M. Hydrogen embrittlement in different materials: a review. Int J Hydrogen Energy 2018;43:21603–16. https://doi.org/10.1016/j.ijhydene.2018.09.201.
[12] Wan C, Liu X, Wang J, Chen F, Cheng D-G. Heterostructuring 2D Co2P nanosheets with 0D CoP via a salt-assisted strategy for boosting hydrogen evolution from ammonia borane hydrolysis. Nano Res 2023;16:6260–9. https://doi.org/10.1007/s12274-023-5388-5.
[13] Wan C, Li G, Wang J, Xu L, Cheng Dg, Chen F, Asakura Y, Kang Y, Yamauchi Y. Modulating electronic metal-support interactions to boost visible-light-driven hydrolysis of ammonia borane: nickel-platinum nanoparticles supported on phosphorus-doped titania. Angew Chem Int Ed 2023;62:e202305371. https://doi.org/10.1002/anie.202305371.
[14] Xu S, Li M, Wang Y, Gao C, Xu R, Jin Z. Enhanced photocatalytic hydrogen production from Co-MOF/CN by nitrogen and sulfur co-doped coal-based carbon quantum dots. J Rare Earths 2024;42:838–50. https://doi.org/10.1016/j.jre.2023.09.020.
[15] Li R-C, Zhang X-Y, Qu Z-Y, Liu F-Y, Xu Q-Q, Hu Z-X, Li J-W, Ghazzal M-N, Yu J-L. One-step controlled electrodeposition nickel sulfides heterointerfaces favoring the desorption of hydroxyl groups for efficient hydrogen generation. Rare Met 2024:1–10. https://doi.org/10.1007/s12598-024-02806-6.
[16] Wan C, Li R, Wang J, Cheng Dg, Chen F, Xu L, Gao M, Kang Y, Eguchi M, Yamauchi Y. Silica confinement for stable and magnetic Co− Cu alloy nanoparticles in nitrogen-doped carbon for enhanced hydrogen evolution. Angew Chem 2024:e202404505. https://doi.org/10.1002/ange.202404505.
[17] Han HG, Choi JW, Son M, Kim KC. Unlocking power of neighboring vacancies in boosting hydrogen evolution reactions on two-dimensional NiPS3 monolayer. eScience 2024;4:100204. https://doi.org/10.1016/j.esci.2023.100204.
[18] Wan C, Liang Y, Zhou L, Huang J, Wang J, Chen F, Zhan X, Cheng D-g. Integration of morphology and electronic structure modulation on cobalt phosphide nanosheets to boost photocatalytic hydrogen evolution from ammonia borane hydrolysis. Green Energy Environ 2022. https://doi.org/10.1016/j.gee.2022.06.007.
[19] Liu W, Niu X, Tang J, Liu Q, Luo J, Liu X, Zhou Y. Energy-efficient anodic reactions for sustainable hydrogen production via water electrolysis. https://dx.doi.org/10.20517/cs.2023.28; 2023.
[20] Abdin Z, Tang C, Liu Y, Catchpole K. Large-scale stationary hydrogen storage via liquid organic hydrogen carriers. iScience 2021;24. https://doi.org/10.1016/j.isci.2021.102966.
[21] Tang J, Su C, Shao Z. Advanced membrane-based electrode engineering toward efficient and durable water electrolysis and cost-effective seawater electrolysis in membrane electrolyzers. Wiley Online Library; 2024, 20220112. https://doi.org/10.1002/EXP.20220112. Exploration.
[22] Rao PC, Yoon M. Potential liquid-organic hydrogen carrier (LOHC) systems: a review on recent progress. Energies 2020;13:6040. https://doi.org/10.3390/en13226040.
[23] Taube M, Rippin D, Cresswell D, Knecht W. A system of hydrogen-powered vehicles with liquid organic hydrides. Int J Hydrogen Energy 1983;8:213–25. https://doi.org/10.1016/0360-3199(83)90067-8.
[24] Meille V, Pitault I. Liquid organic hydrogen carriers or organic liquid hydrides: 40 years of history. Reactions 2021;2:94–101. https://doi.org/10.3390/reactions2020008.
[25] Sultan O, Shaw H. Study of automotive storage of hydrogen using recyclable liquid chemical carriers [Catalytic dehydrogenation of naphthenes]. Exxon Research and Engineering Co., Linden, NJ. USA: Government Research Lab; 1975.
[26] Parmaliana A, Crisafulli C, Maggiore R, Bart J, Giordano N. Catalytic activity of honeycomb catalysts, I. The benzene-cyclohexane (de) hydrogenation reaction. React Kinet Catal Lett 1981;18:295–9.
[27] Taube M, Taube P. A liquid organic carrier of hydrogen as a fuel for automobiles. Eidgenoessisches Inst. fuer Reaktorforschung; 1979.
[28] Bélanger G. Cyclohexane, a liquid hydride. Adv Hydrogen Energy 1982;3:1335–43.
[29] Taube M, Rippin D, Knecht W, Hakimifard D, Milisavljevic B, Gruenenfelder N. A prototype truck powered by hydrogen from organic liquid hydrides. Int J Hydrogen Energy 1985;10:595–9. https://doi.org/10.1016/0360-3199(85)90035-7.
[30] Grünenfelder N, Schucan TH. Seasonal storage of hydrogen in liquid organic hydrides: description of the second prototype vehicle. Int J Hydrogen Energy 1989;14:579–86. https://doi.org/10.1016/0360-3199(89)90117-1.
[31] Cooper AC, Campbell KM, Pez GP. An integrated hydrogen storage and delivery approach using organic liquid-phase carriers. In: Proceedings of the 16th world hydrogen energy conference; 2006. p. 13–6. Lyon, France.
[32] Cooper AC, Campbell KM, Pez GP. An integrated hydrogen storage and delivery approach using organic liquid-phase carriers. In: Proc 16th world hydrogen energy conference; 2006. Lyon, France.
[33] Morawa Eblagon K, Tam K, Yu KK, Zhao S-L, Gong X-Q, He H, Ye L, Wang L-C, Ramirez-Cuesta AJ, Tsang SC. Study of catalytic sites on ruthenium for hydrogenation of N-ethylcarbazole: implications of hydrogen storage via reversible catalytic hydrogenation. J Phys Chem C 2010;114:9720–30. https://doi.org/10.1021/jp908640k.
[34] Fan Y, Wang P, Zhang J, Huang M, Liu W, Xu Y, Duan X, Li Y, Zhang J. Continuous hydrogenation of N-ethylcarbazole in a micro-packed bed reactor for hydrogen storage. Chem Eng J 2024;484:149404. https://doi.org/10.1016/j.cej.2024.149404.
[35] Yadav V, Sivakumar G, Gupta V, Balaraman E. Recent advances in liquid organic hydrogen carriers: an alcohol-based hydrogen economy. ACS Catal 2021;11:14712–26. https://doi.org/10.1021/acscatal.1c03283.
[36] Zhou L, Sun L, Xu L, Wan C, An Y, Ye M. Recent developments of effective catalysts for hydrogen storage technology using N-Ethylcarbazole. Catalysts 2020;10:648. https://doi.org/10.3390/catal10060648.
[37] Singh R, Singh M, Gautam S. Hydrogen economy, energy, and liquid organic carriers for its mobility. Mater Today Proc 2021;46:5420–7. https://doi.org/10.1016/j.matpr.2020.09.065.
[38] Yang M, Dong Y, Fei S, Ke H, Cheng H. A comparative study of catalytic dehydrogenation of perhydro-N-ethylcarbazole over noble metal catalysts. Int J Hydrogen Energy 2014;39:18976–83. https://doi.org/10.1016/j.ijhydene.2014.09.123.
[39] Eblagon KM, Rentsch D, Friedrichs O, Remhof A, Zuettel A, Ramirez-Cuesta A, Tsang SC. Hydrogenation of 9-ethylcarbazole as a prototype of a liquid hydrogen carrier. Int J Hydrogen Energy 2010;35:11609–21. https://doi.org/10.1016/j.ijhydene.2010.03.068.
[40] Sobota M, Nikiforidis I, Amende M, Zanón BS, Staudt T, Höfert O, Lykhach Y, Papp C, Hieringer W, Laurin M. Dehydrogenation of dodecahydro-N-ethylcarbazole on Pd/Al2O3 model catalysts. Chem–Eur J 2011;17:11542–52. https://doi.org/10.1002/chem.201101311.
[41] Hu P, Fogler E, Diskin-Posner Y, Iron MA, Milstein D. A novel liquid organic hydrogen carrier system based on catalytic peptide formation and hydrogenation. Nat Commun 2015;6:1–7. https://doi.org/10.1038/ncomms7859.

[42] Forberg D, Schwob T, Zaheer M, Friedrich M, Miyajima N, Kempe R. Single-catalyst high-weight% hydrogen storage in an N-heterocycle synthesized from lignin hydrogenolysis products and ammonia. Nat Commun 2016;7:1–6. https://doi.org/10.1038/ncomms13201.
[43] Amende M, Gleichweit C, Schernich S, Höfert O, Lorenz MP, Zhao W, Koch M, Obesser K, Papp C, Wasserscheid P. Size and structure effects controlling the stability of the liquid organic hydrogen carrier dodecahydro-N-ethylcarbazole during dehydrogenation over Pt model catalysts. The journal of physical chemistry letters 2014;5:1498–504. https://doi.org/10.1021/jz500157r.
[44] Niermann M, Beckendorff A, Kaltschmitt M, Bonhoff K. Liquid organic hydrogen carrier (LOHC)–Assessment based on chemical and economic properties. Int J Hydrogen Energy 2019;44:6631–54. https://doi.org/10.1016/j.ijhydene.2019.01.199.
[45] Sotoodeh F, Smith KJ. An overview of the kinetics and catalysis of hydrogen storage on organic liquids. Can J Chem Eng 2013;91:1477–90. https://doi.org/10.1002/cjce.21871.
[46] Jorschick H, Geißelbrecht M, Eßl M, Preuster P, Bösmann A, Wasserscheid P. Benzyltoluene/dibenzyltoluene-based mixtures as suitable liquid organic hydrogen carrier systems for low temperature applications. Int J Hydrogen Energy 2020;45:14897–906. https://doi.org/10.1016/j.ijhydene.2020.03.210.
[47] Jorschick H, Preuster P, Dürr S, Seidel A, Müller K, Bösmann A, Wasserscheid P. Hydrogen storage using a hot pressure swing reactor. Energy Environ Sci 2017;10:1652–9. https://doi.org/10.1039/C7EE00476A.
[48] Jorschick H, Dürr S, Preuster P, Bösmann A, Wasserscheid P. Operational stability of a LOHC-based hot pressure swing reactor for hydrogen storage. Energy Technol 2019;7:146–52. https://doi.org/10.1002/ente.201800499.
[49] Fikrt A, Brehmer R, Milella V-O, Müller K, Bösmann A, Preuster P, Alt N, Schlücker E, Wasserscheid P, Arlt W. Dynamic power supply by hydrogen bound to a liquid organic hydrogen carrier. Applied energy 2017;194:1–8. https://doi.org/10.1016/j.apenergy.2017.02.070.
[50] Yolcular S, Olgun Ö. Hydrogen storage in the form of methylcyclohexane. Energy Sources, Part A Recovery, Util Environ Eff 2007;30:149–56. https://doi.org/10.1080/00908310600712315.
[51] Sebastián D, Bordejé E, Calvillo L, Lazaro M, Moliner R. Hydrogen storage by decalin dehydrogenation/naphthalene hydrogenation pair over platinum catalysts supported on activated carbon. Int J Hydrogen Energy 2008;33:1329–34. https://doi.org/10.1016/j.ijhydene.2007.12.037.
[52] Modisha PM, Ouma CN, Garidzirai R, Wasserscheid P, Bessarabov D. The prospect of hydrogen storage using liquid organic hydrogen carriers. Energy & fuels 2019;33:2778–96. https://doi.org/10.1021/acs.energyfuels.9b00296.
[53] Cacciola G, Giordano N, Restuccia G. Cyclohexane as a liquid phase carrier in hydrogen storage and transport. Int J Hydrogen Energy 1984;9:411–9. https://doi.org/10.1016/0360-3199(84)90062-4.
[54] Müller K, Stark K, Müller B, Arlt W. Amine borane based hydrogen carriers: an evaluation. Energy & fuels 2012;26:3691–6. https://doi.org/10.1021/ef300516m.
[55] Müller K, Völkl J, Arlt W. Thermodynamic evaluation of potential organic hydrogen carriers. Energy Technol 2013;1:20–4. https://doi.org/10.1002/ente.201200045.
[56] Xie Y, Milstein D. Pd catalyzed, acid accelerated, rechargeable, liquid organic hydrogen carrier system based on methylpyridines/methylpiperidines. ACS Appl Energy Mater 2019;2:4302–8. https://doi.org/10.1021/acsaem.9b00523.
[57] Tan KC, He T, Chua YS, Chen P. Recent advances of catalysis in the hydrogenation and dehydrogenation of N-heterocycles for hydrogen storage. J Phys Chem C 2021;125:18553–66. https://doi.org/10.1021/acs.jpcc.1c04783.
[58] Sotoodeh F, Zhao L, Smith KJ. Kinetics of H2 recovery from dodecahydro-N-ethylcarbazole over a supported Pd catalyst. Appl Catal Gen 2009;362:155–62. https://doi.org/10.1016/j.apcata.2009.04.039.
[59] Amende M, Gleichweit C, Werner K, Schernich S, Zhao W, Lorenz MP, Höfert O, Papp C, Koch M, Wasserscheid P. Model catalytic studies of liquid organic hydrogen carriers: dehydrogenation and decomposition mechanisms of dodecahydro-N-ethylcarbazole on Pt (111). ACS Catal 2014;4:657–65. https://doi.org/10.1021/cs400946x.
[60] Amende M, Schernich S, Sobota M, Nikiforidis I, Hieringer W, Assenbaum D, Gleichweit C, Drescher HJ, Papp C, Steinrück HP. Dehydrogenation mechanism of liquid organic hydrogen carriers: dodecahydro-N-ethylcarbazole on Pd (111). Chem–Eur J 2013;19:10854–65. https://doi.org/10.1002/chem.201301323.
[61] Sotoodeh F, Smith KJ. Analysis of H2 release from organic polycyclics over Pd catalysts using DFT. J Phys Chem C 2013;117:194–204. https://doi.org/10.1021/jp307325s.
[62] Tang C, Permude P, Fei S, Frankcombe TJ, Smith SC, Liu Y. Critical dehydrogenation steps of perhydro-N-ethylcarbazole on Ru (0001) surface. Comput Mater Sci 2023;229:112373. https://doi.org/10.1016/j.commatsci.2023.112373.
[63] Gleichweit C, Amende M, Schernich S, Zhao W, Lorenz M, Höfert O, Brückner N, Wasserscheid P, Libuda J, Steinrück HP. Dehydrogenation of dodecahydro-N-ethylcarbazole on Pt (111). ChemSusChem 2013;6. https://doi.org/10.1002/cssc.201300263.
[64] Gleichweit C, Amende M, Schernich S, Zhao W, Lorenz MP, Höfert O, Brückner N, Wasserscheid P, Libuda J, Steinrück HP. Dehydrogenation of dodecahydro-N-ethylcarbazole on Pt (111). ChemSusChem 2013;6:974–7.
[65] Papp C. In-situ investigations of adsorbed hydrocarbons-model systems of heterogeneous catalysis: friedrich-Alexander-Universitaet Erlangen-Nuernberg (Germany). 2007.
[66] Ihm H, White J. Stepwise dissociation of thermally activated phenol on Pt (111). J Phys Chem B 2000;104:6202–11. https://doi.org/10.1021/jp0005423.
[67] Wang B, Li P-y, Wang S-y, Lu S-h, Fang T. Tuning the interaction between Pd and MgAl2O4 to enhance the dehydrogenation activity and selectivity of dodecahydro-N-ethylcarbazole. ACS Sustainable Chem Eng 2023. https://doi.org/10.1021/acssuschemeng.2c07039.
[68] Jiang Z, Gong X, Wang B, Wu Z, Fang T. A experimental study on the dehydrogenation performance of dodecahydro-N-ethylcarbazole on M/TiO2 catalysts. Int J Hydrogen Energy 2019;44:2951–9. https://doi.org/10.1016/j.ijhydene.2018.11.236.
[69] Wan C, An Y, Xu G, Kong W. Study of catalytic hydrogenation of N-ethylcarbazole over ruthenium catalyst. Int J Hydrogen Energy 2012;37:13092–6. https://doi.org/10.1016/j.ijhydene.2012.04.123.
[70] Preuster P, Papp C, Wasserscheid P. Liquid organic hydrogen carriers (LOHCs): toward a hydrogen-free hydrogen economy. Accounts of chemical research 2017;50:74–85. https://doi.org/10.1021/acs.accounts.6b00474.
[71] Ye X, An Y, Xu G. Kinetics of 9-ethylcarbazole hydrogenation over Raney-Ni catalyst for hydrogen storage. J Alloys Compd 2011;509:152–6. https://doi.org/10.1016/j.jallcom.2010.09.012.
[72] Sun F, An Y, Lei L, Wu F, Zhu J, Zhang X. Identification of the starting reaction position in the hydrogenation of (N-ethyl) carbazole over Raney-Ni. J Energy Chem 2015;24:219–24. https://doi.org/10.1016/S2095-4956(15)60304-7.
[73] Eblagon KM, Tam K, Yu K, Tsang S. Comparative study of catalytic hydrogenation of 9-ethylcarbazole for hydrogen storage over noble metal surfaces. J Phys Chem C 2012;116:7421–9. https://doi.org/10.1021/jp212249g.
[74] Eblagon KM, Tam K, Tsang SCE. Comparison of catalytic performance of supported ruthenium and rhodium for hydrogenation of 9-ethylcarbazole for hydrogen storage applications. Energy Environ Sci 2012;5:8621–30. https://doi.org/10.1039/C2EE22066K.
[75] Wan C, An Y, Chen F, Cheng D, Wu F, Xu G. Kinetics of N-ethylcarbazole hydrogenation over a supported Ru catalyst for hydrogen storage. Int J Hydrogen Energy 2013;38:7065–9. https://doi.org/10.1016/j.ijhydene.2013.04.022.
[76] Sotoodeh F, Smith KJ. Kinetics of hydrogen uptake and release from heteroaromatic compounds for hydrogen storage. Ind Eng Chem Res 2010;49:1018–26. https://doi.org/10.1021/ie9007002.
[77] Gianotti E, Taillades-Jacquin Ml, Rozière J, Jones DJ. High-purity hydrogen generation via dehydrogenation of organic carriers: a review on the catalytic process. ACS Catal 2018;8:4660–80. https://doi.org/10.1021/acscatal.7b04278.
[78] Tritsaris GA, Nørskov JK, Rossmeisl J. Trends in oxygen reduction and methanol activation on transition metal chalcogenides. Electrochim Acta 2011;56:9783–8. https://doi.org/10.1016/j.electacta.2011.08.045.
[79] Makaryan I, Sedov I. Hydrogenation/dehydrogenation catalysts for hydrogen storage systems based on liquid organic carriers (A review). Petrol Chem 2021;61:977–88. https://doi.org/10.1134/S0965544121090085.
[80] Lu H, Hou L, Zhang Y, Cao X, Xu X, Shang Y. Pilot-scale and large-scale Fenton-like applications with nano-metal catalysts: from catalytic modules to scale-up applications. Water Res 2024:122425. https://doi.org/10.1016/j.watres.2024.122425.
[81] Qin Y, Shi J, Bai X. Preparing ultra-stable Ru nanocatalysts supported on partially graphitized biochar via carbothermal reduction for hydrogen storage of N-ethylcarbazole. Int J Hydrogen Energy 2021;46:25543–54. https://doi.org/10.1016/j.ijhydene.2021.05.074.
[82] Shi J, Liu X, Bai X. Effect of N-doping, exfoliation, defect-inducing of Ni-Fe layered double hydroxide (Ni-Fe LDH) nanosheets on catalytic hydrogen storage of N-ethylcarbazole over Ru/Ni-Fe LDH. Fuel 2021;306:121688. https://doi.org/10.1016/j.fuel.2021.121688.
[83] Liu H, Zhou C, Li W, Li W, Qiu M, Chen X, Wang H, Sun Y. Ultralow Rh bimetallic catalysts with high catalytic activity for the hydrogenation of N-ethylcarbazole. ACS Sustainable Chem Eng 2021;9:5260–7. https://doi.org/10.1021/acssuschemeng.0c08270.
[84] Wu Y, Yu H, Guo Y, Zhang Y, Jiang X, Sun B, Fu K, Chen J, Qi Y, Zheng J. Promoting hydrogen absorption of liquid organic hydrogen carriers by solid metal hydrides. J Mater Chem A 2019;7:16677–84. https://doi.org/10.1039/C9TA05966K.
[85] Ding Y, Dong Y, Zhang H, Zhao Y, Yang M, Cheng H. A highly adaptable Ni catalyst for Liquid Organic Hydrogen Carriers hydrogenation. Int J Hydrogen Energy 2021;46:27026–36. https://doi.org/10.1016/j.ijhydene.2021.05.196.
[86] Wang B, Li P-y, Dong Q, Chen L-q, Wang H-q, Han P-l, Fang T. Bimetallic NiCo/AC catalysts with a strong coupling effect for high-efficiency hydrogenation of N-ethylcarbazole. ACS Appl Energy Mater 2023;6:1741–52. https://doi.org/10.1021/acsaem.2c03630.
[87] Wang B, Wang S-y, Lu S-h, Li P-y, Fang T. Trace ultrafine Ru nanoparticles on Ni/Al hydrotalcite-derived oxides supports as extremely active catalysts for N-ethylcarbazole hydrogenation. Fuel 2023;339:127338. https://doi.org/10.1016/j.ijhydene.2021.05.196.
[88] Jiang Z, Guo S, Fang T. Enhancing the catalytic activity and selectivity of PdAu/SiO2 bimetallic catalysts for dodecahydro-N-ethylcarbazole dehydrogenation by controlling the particle size and dispersion. ACS Appl Energy Mater 2019;2:7233–43. https://doi.org/10.1021/acsaem.9b01202.
[89] Wang B, Chen Y-T, Chang T-Y, Jiang Z, Huang Z-Q, Wang S-Y, Chang C-R, Chen Y-S, Wei J-J, Yang S. Facet-dependent catalytic activities of Pd/rGO: exploring dehydrogenation mechanism of dodecahydro-N-ethylcarbazole. Applied Catalysis B: Environmental. 2020;266:118658. https://doi.org/10.1016/j.apcatb.2020.118658.
[90] Jiang Z, Gong X, Guo S, Bai Y, Fang T. Engineering PdCu and PdNi bimetallic catalysts with adjustable alloying degree for the dehydrogenation reaction of dodecahydro-N-ethylcarbazole. Int J Hydrogen Energy 2021;46:2376–89. https://doi.org/10.1016/j.ijhydene.2020.10.123.

[91] Wang B, Chang T-y, Jiang Z, Wei J-j, Fang T. Component controlled synthesis of bimetallic PdCu nanoparticles supported on reduced graphene oxide for dehydrogenation of dodecahydro-N-ethylcarbazole. Applied Catalysis B: Environmental. 2019;251:261–72. https://doi.org/10.1016/j.apcatb.2019.03.071.
[92] Shuang H, Chen H, Wu F, Li J, Cheng C, Li H, Fu J. Catalytic dehydrogenation of hydrogen-rich liquid organic hydrogen carriers by palladium oxide supported on activated carbon. Fuel 2020;275:117896. https://doi.org/10.1016/j.fuel.2020.117896.
[93] Wang B, Yan T, Chang T, Wei J, Zhou Q, Yang S, Fang T. Palladium supported on reduced graphene oxide as a high-performance catalyst for the dehydrogenation of dodecahydro-N-ethylcarbazole. Carbon 2017;122:9–18. https://doi.org/10.1016/j.carbon.2017.06.021.
[94] Zhu M, Xu L, Du L, An Y, Wan C. Palladium supported on carbon nanotubes as a high-performance catalyst for the dehydrogenation of dodecahydro-N-ethylcarbazole. Catalysts 2018;8:638. https://doi.org/10.3390/catal8120638.
[95] Li X, Wu F, Zhou W, Chen C, Wang J, Li B, Chen H, Fu J. Low-temperature dehydrogenation of dodecahydro-N-ethylcarbazole catalyzed by PdCo bimetallic oxide. Chem Eng Sci 2023;273:118650. https://doi.org/10.1016/j.ces.2023.118650.
[96] Gong X, Jiang Z, Fang T. Enhancing selectivity and reducing cost for dehydrogenation of dodecahydro-N-ethylcarbazole by supporting platinum on titanium dioxide. Int J Hydrogen Energy 2020;45:6838–47. https://doi.org/10.1016/j.ijhydene.2019.12.203.
[97] Peters W, Seidel A, Herzog S, Bösmann A, Schwieger W, Wasserscheid P. Macrokinetic effects in perhydro-N-ethylcarbazole dehydrogenation and H 2 productivity optimization by using egg-shell catalysts. Energy Environ Sci 2015;8:3013–21. https://doi.org/10.1039/C5EE02024G.
[98] Tarasov AL, Tkachenko OP, Kustov LM. Mono and bimetallic Pt–(M)/Al2O3 catalysts for dehydrogenation of perhydro-N-ethylcarbazole as the second stage of hydrogen storage. Catal Lett 2018;148:1472–7. https://doi.org/10.1007/s10562-018-2325-4.
[99] Li L, Gong X, Yang Z, Zhang R, Jiang Z, Fang T. Boosting the dehydrogenation efficiency of dodecahydro-N-ethylcarbazole by assembling Pt nanoparticles on the single-layer Ti3C2Tx MXene. Int J Hydrogen Energy 2023. https://doi.org/10.1016/j.ijhydene.2023.02.048.
[100] Garcia-Baldovi A, Peng L, Dhakshinamoorthy A, Asiri AM, Primo A, Garcia H. Positive influence of minute Pt addition on the activity of Ni supported on defective graphene for hydrogenation/dehydrogenation of N-ethylcarbazole as liquid organic carrier. Catal Commun 2023;177:106641. https://doi.org/10.1016/j.catcom.2023.106641.
[101] Wang B, Chang T-y, Jiang Z, Wei J-j, Zhang Y-h, Yang S, Fang T. Catalytic dehydrogenation study of dodecahydro-N-ethylcarbazole by noble metal supported on reduced graphene oxide. Int J Hydrogen Energy 2018;43:7317–25. https://doi.org/10.1016/j.ijhydene.2018.02.156. 10.1016/j.ijhydene.2018.02.156.
[102] Feng Z, Chen X, Bai X. Catalytic dehydrogenation of liquid organic hydrogen carrier dodecahydro-N-ethylcarbazole over palladium catalysts supported on different supports. Environ Sci Pollut Res Int 2020;27:36172–85. https://doi.org/10.1007/s11356-020-09698-w. 10.1007/s11356-020-09698-w.
[103] Feng Z, Chen X, Bai X. Catalytic dehydrogenation of liquid organic hydrogen carrier dodecahydro-N-ethylcarbazole over palladium catalysts supported on different supports. Environ Sci Pollut Control Ser 2020;27:36172–85. https://doi.org/10.1007/s11356-020-09698-w.
[104] Wu Y, Yu H, Guo Y, Jiang X, Qi Y, Sun B, Li H, Zheng J, Li X. A rare earth hydride supported ruthenium catalyst for the hydrogenation of N-heterocycles: boosting the activity via a new hydrogen transfer path and controlling the stereoselectivity. Chem Sci 2019;10:10459–65. https://doi.org/10.1039/C9SC04365A. 10.1039/c9sc04365a.
[105] Yang X, Wu Y, Yu H, Sun M, Zheng J, Li X, Lin W, Wu Y. A YH3 promoted palladium catalyst for reversible hydrogen storage of N-ethylcarbazole. Int J Hydrogen Energy 2020;45:33657–62. https://doi.org/10.1016/j.ijhydene.2020.09.043.
[106] Yu H, Yang X, Wu Y, Guo Y, Li S, Lin W, Li X, Zheng J. Bimetallic Ru-Ni/TiO2 catalysts for hydrogenation of N-ethylcarbazole: role of TiO2 crystal structure. J Energy Chem 2020;40:188–95. https://doi.org/10.1016/j.jechem.2019.04.009. 10.1016/j.jechem.2019.04.009.
[107] Yu H, Yang X, Jiang X, Wu Y, Chen S, Lin W, Wu Y, Xie L, Li X, Zheng J. LaNi5. 5 particles for reversible hydrogen storage in N-ethylcarbazole. Nano Energy 2021;80:105476. https://doi.org/10.1016/j.nanoen.2020.105476.
[108] Xue W, Liu H, Mao B, Liu H, Qiu M, Yang C, Chen X, Sun Y. Reversible hydrogenation and dehydrogenation of N-ethylcarbazole over bimetallic Pd-Rh catalyst for hydrogen storage. Chem Eng J 2021;421. https://doi.org/10.1016/j.cej.2020.127781. 10.1016/j.cej.2020.127781.
[109] Xue W, Liu H, Zhao B, Ge L, Yang S, Qiu M, Li J, Han W, Chen X. Single Rh1Co catalyst enabling reversible hydrogenation and dehydrogenation of N-ethylcarbazole for hydrogen storage. Applied Catalysis B: Environmental. 2023;327:122453. https://doi.org/10.1016/j.apcatb.2023.122453.
[110] Cheng N, Zhang L, Doyle-Davis K, Sun X. Single-atom catalysts: from design to application. Electrochem Energy Rev 2019;2:539–73. https://doi.org/10.1007/s41918-019-00050-6.
[111] Zhang J, Wang W, Chen X, Jin J, Yan X, Huang J. Single-atom Ni supported on TiO2 for catalyzing hydrogen storage in MgH2. J Am Chem Soc 2024;146:10432–42. https://doi.org/10.1021/jacs.3c13970?urlappend=%3Fref%3DPDF&jav=VoR&rel=cite-as.
[112] Bagi S, Yuan S, Rojas-Buzo S, Shao-Horn Y, Román-Leshkov Y. A continuous flow chemistry approach for the ultrafast and low-cost synthesis of MOF-808. Green Chem 2021;23:9982–91. https://doi.org/10.1039/D1GC02824C.